Louisiana State University
LSU Digital Commons

LSU Doctoral Dissertations | Graduate School

3-26-2021

Non-Newtonian Model Development for Post-Wildfire Flood Risk Management

Ian Eli Floyd

Follow this and additional works at: https://digitalcommons.lsu.edu/gradschool_dissertations

 Part of the Civil Engineering Commons, and the Hydraulic Engineering Commons

Recommended Citation

Floyd, Ian Eli, "Non-Newtonian Model Development for Post-Wildfire Flood Risk Management" (2021). *LSU Doctoral Dissertations*. 5513.
https://digitalcommons.lsu.edu/gradschool_dissertations/5513

This Dissertation is brought to you for free and open access by the Graduate School at LSU Digital Commons. It has been accepted for inclusion in LSU Doctoral Dissertations by an authorized graduate school editor of LSU Digital Commons. For more information, please contactgradetd@lsu.edu.

NON-NEWTONIAN MODEL DEVELOPMENT FOR POST-WILDFIRE FLOOD RISK MANAGEMENT

A Dissertation

Submitted to the Graduate Faculty of the
Louisiana State University and
Agricultural and Mechanical College
in partial fulfillment of the
requirements for the degree of
Doctor of Philosophy

in

The Donald W. Clayton Graduate Program in Engineering Science

by
Ian Eli Floyd
B.S., University of Southern Mississippi, 2008
M.S., University of Southern Mississippi, 2010
May 2021

ACKNOWLEDGEMENTS

First and foremost I would like to thank my better half Claire for her unwavering support in pursuing my PhD – from Long Term Training, symptoms of PTSD, a topic change, the birth of our first child (Walker), to completion of my dissertation. Without her I would not be writing this today. She has been unwavering of her support for me and provides a cherished constant in my life. Secondly, I would like to thank my mother, Mrs. Theresa Floyd, and brother, Dr. Tyler Floyd, for their loving support and countless incredible moments over the years. Ours was not an easy life, but we made it together. I know dad would be proud. Thirdly, I would like to thank my co-Chairs Clint Willson and Sam Bentley for taking a chance on me all those years ago. They are both true gentlemen and scholars. I would also like to thank Dr. Jane Smith for her guidance and support. Additionally, I would like to thank Dr. David Wheat, Dr. Robert Lundy, and the ladies of Hinds Behavioral Health Services Region 9 with my struggles with PTSD and mental health.

I have many work colleagues that have helped throughout the dissertation processes I wish to thank. Specifically, I want to give a special thanks to Mr. Ronald Heath, Dr. Travis Dahl, Dr. Gaurav Savant, Dr. Stanford Gibson, Dr. Nawa Pradhan, and Dr. Alejandro Sanchez for their assistance and support during this effort. I would also like to thank the USACE Civil Work R&D lead Dr. Julie Rosati for her continued funding and support of my research over the years. This research was supported by a research work unit of the U.S. Army Corps of Engineer's Flood and Coastal Systems Storm Damage Reduction (F&CS) research program, specifically Flood Risk Management. Information for the F&CS program can be found at https://chl.erdc.dren.mil/civil-works/mission-areas/flood-risk-management/.

TABLE OF CONTENTS

ABSTRACT

Wildfire effected regions of the western U.S. frequently produce non-Newtonian floods (or floods that have a non-linear relationship between stress and deformation) in response to moderate to severe precipitation events. This research presents the development, evaluation, and demonstration of a post-wildfire hydrodynamic one-dimensional and two-dimensional diffusive wave and shallow-water numerical modeling approach that can be used to predict post-wildfire downstream runout of debris flows and floodplain inundation conditions. While researchers have developed a variety of Non-Newtonian approaches to simulate debris flows and mudflows, there has been very limited application to post-wildfire flooding. This can make it difficult to understand the assumptions and limitations in any given model or replicate work, making the modular non-Newtonian computation library approach presented in this dissertation advantageous. This research was conducted with two widely used U.S. Army Corp of Engineer's (USACE) hydraulic modeling software: the two-dimensional Hydraulic Engineering Center (HEC) River Analysis System (HEC-RAS); and the two-dimensional Adaptive Hydraulics (AdH). First, this research demonstrates the effectiveness of the non-Newtonian library, DebrisLib, to predict a variety of non-Newtonian flow conditions using flume experiments from Hungr (1995), Haldenwang (2003), and Iverson et al. (2010). The modeling approach was then validated using Kean et al. (2019) datasets collected following the 2017 Thomas Fire and 09 January 2019 post-wildfire debris flow events near Santa Barbara, California. The evaluation of the numerical modeling approaches versus observed laboratory and field data indicates that both HEC-RAS and AdH, when linked with the non-Newtonian library DebrisLib, can adequately predict a range of non-Newtonian flow conditions. The shallow-water hydraulic models with non-Newtonian library DebrisLib were able to replicate the downstream runout and floodplain inundation demonstrating the effectiveness of the numerical modeling framework. The results

from both flume and the 09 January 2019 flood events demonstrates that Newtonian physics-based models are not capable of predicting these types of events. The post-wildfire non-Newtonian approaches presented here provide an improvement to the existing state-of-practice for predicting post-wildfire flood risk, specifically, the ability to predict downstream runout and floodplain inundation.

CHAPTER 1. NON-NEWTONIAN MODEL DEVELOPMENT FOR POST-WILDFIRE FLOOD RISK MANAGEMENT

1.1 INTRODUCTION

In the southwestern U.S., disastrous flood events are usually the result of heavy rainfall. In these regions, wildfires are a natural (and human-induced) impact that may significantly contribute to the flood risks (DeBano et al., 1998; Neary et al., 2005; Moody et al., 2013). The arid and semi-arid physiographic regions of the southwestern U.S. have unique and severe flooding and river restoration problems. The region has rapidly developing population centers and unique watershed management concerns, with post-wildfire flood risk management becoming an urgent problem for federal, state, regional, and local land management agencies. This is especially serious in the western U.S. where storms are infrequent but often highly intense, which is more likely to cause severe damage to vital ecosystems and to increase risks to life, property, and critical infrastructure.

Immediately following a wildfire, vegetation is removed, organic soil horizons are reduced to ash, and soils may have turned hydrophobic, which combine to result in increased surface runoff, water and sediment discharge, and debris, mud, and hyperconcentrated flows (Moody et al., 2013). In the years following a wildfire, ecotone shifts, gully formation, and channel incision alter the hydrologic system response, resulting in dramatic changes in hydraulic and sediment impacts down system. Wildfires represent a significant perturbation to natural systems that dramatically alter the morphological, hydrology and sediment regimes of impacted watersheds. Surface runoff and debris flow processes in burned watersheds are complex processes and are poorly understood quantitatively (Moody et al., 2013). Post-wildfire non-Newtonian (i.e. debris flow, mudflow) floods are a common response following wildfires in the western U.S. (Bernard, 2007; Cannon et al., 2010; Moody et al., 2013; Kean et al., 2019). Non-Newtonian debris flow

models can be useful for assessing wildfire impacts but are currently not broadly applied within the flood risk management community (Moody et al., 2013; Kean et al., 2019). There is an increasing need to continue development of non-Newtonian numerical modeling capabilities within widely available one-dimensional and two-dimensional diffusive wave and shallow-water hydraulic numerical models. In addition, there are large numbers of existing hydrodynamic models within the engineering and flood risk community which could be used or adapted to take post-wildfire non-Newtonian flows into account. As presented in this research, the addition of a post-wildfire and non-Newtonian module to existing hydraulic and hydrologic numerical model software will allow users to quickly extend existing models to simulate post-wildfire non-Newtonian flows, thus improving predictions and saving time and money. This dissertation will address the following basic questions:

1) What are the dominant non-Newtonian processes needed to predict non-Newtonian flow conditions within Newtonian hydrodynamic numerical models? Can a modular non-Newtonian numerical model library approach improve upon existing state-of-knowledge shallow-water and diffusive wave Newtonian models?

2) How effective are existing non-Newtonian rheology models (e.g., Bingham, HB, and Quadratic) at predicting non-Newtonian turbulent, transitional, and laminar flow conditions?

3) Can non-Newtonian rheology-based closure approaches within hydrodynamic models decrease uncertainty in predicting the downstream runout and inundation and flow variability associated with post-wildfire flood events?

The main goal of this research is to establish a physically realistic numerical modeling framework that can be used to simulate post-wildfire non-Newtonian flood events to assess

the risk in downstream communities. Two U.S. Army Corp of Engineers numerical software packages are used in this research: two-dimensional Adaptive Hydraulics (AdH) and one-dimensional and two-dimensional Hydrologic Engineering Center River Analysis System (HEC-RAS). The models are applied to a recent flume and field data in order to assess: 1) the limitations of current rheology-based non-Newtonian approaches within shallow-water models; 2) the applicability of finite-volume and finite-element numerical models for predicting post-wildfire stream flow by comparing measured data with simulations; and 3) the role of non-Newtonian behavior on overall post-wildfire stream flow by comparing simulation to measured field data (Kean et al., 2019).

1.2. OVERVIEW AND APPROACH

The research presented here is focused on addressing engineering challenges associated with prediction of post-wildfire non-Newtonian flood response within one-dimensional and two-dimensional hydrology and hydraulic numerical models. Evaluation and improvement of post-wildfire non-Newtonian flood runout and inundation capabilities is assessed through the use of various non-Newtonian flume experiment data (e.g., Hungr, 1995; Haldenwang, 2003; Iverson, 1997) and the 2017 Thomas Fire post-wildfire flooding datasets. This research was accomplished through the following: a comprehensive literature review, development of a modular Non-Newtonian model library development, data gathering and evaluation, and model verification and validation as shown in Figure 1.

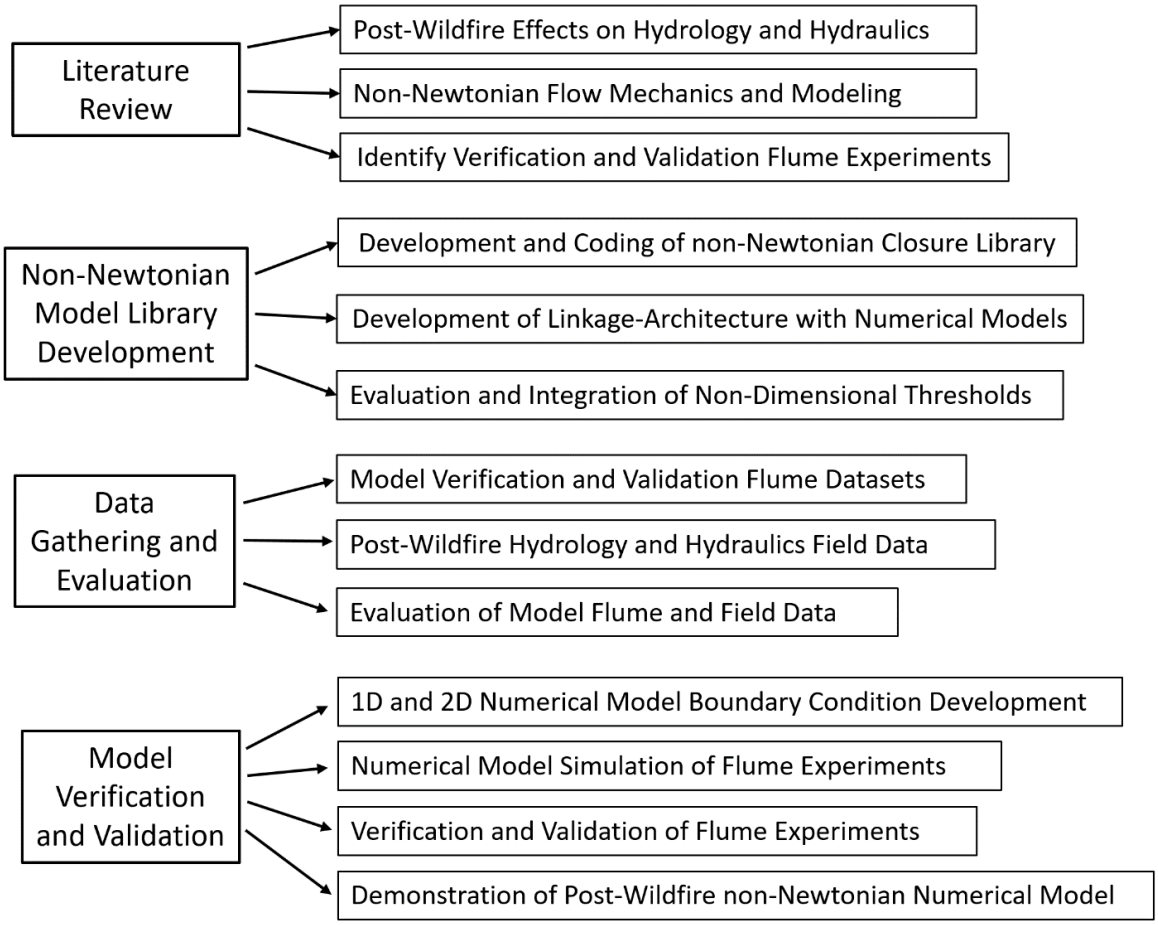

Figure 1. Research approach and outline.

Chapter One presents an introduction, background, overview of the research needs and questions, research objectives.

Chapter Two presents the development and validation of a modular non-Newtonian library that modifies existing diffusive wave equation (DWE) and shallow-water equation (SWE) numerical software to predict non-Newtonian behavior associated with post-wildfire flooding. The non-Newtonian library 'DebrisLib' theory, background, and implementation are demonstrated using the one- and two-dimensional HEC-RAS models and the two-dimensional AdH numerical model. The validity of the non-Newtonian model closure was confirmed using multiple flume experiments over a range of sediment gradations, sediment concentrations, and flow conditions. The flume experiments used in this research include: Hungr (1995), Haldenwang (2003), and the

USGS Large Scale Experiment Flume (Iverson et al., 2010). The companion paper Gibson et al. (2020) extends the DebrisLib approach to flume experiments conducted by Parson et al. (2001) for higher concentrated (> 50% volumetric concentration) mudflows and debris flows.

Chapter Three focuses on evaluation and prediction of turbulent and laminar non-Newtonian flow conditions through comparison of the two-dimensional HEC-RAS and AdH numerical models, linked with DebrisLib, against the Haldenwang (2003) flume experiments. The aim is to evaluate how effective rheology-based approaches are at predicting turbulent and laminar flows for lower suspended sediment concentration (or hyperconcentrated) flows. A selection of flume experiments using 10% volumetric concentrated mixtures of kaolinite were simulated using the two-dimensional hydraulic models HEC-RAS and AdH. Validation was conducted by comparison between measured and modeled results of discharge and depth. The relatively small residuals between measured and predicted flow-depth curves indicate the validity of the application of the DebrisLib library for modifying Newtonian models to account for the documented non-Newtonian behavior.

Chapter Four presents a hydrology and hydraulic post-wildfire conceptual modeling framework and demonstrates the effectiveness of the non-Newtonian modeling approach at predicting a real-world post-wildfire flood event following the 2017 Thomas Fire near Santa Barbara, California. The primary focus of this chapter is to evaluate and validate the non-Newtonian hydraulic modeling of downstream runout and floodplain inundation using post-flood data collected by Kean et al. (2019). The approach attempts to balance the need and demand for engineering-based numerical models with the level of model complexity, computation demand, and uncertainty. This is accomplished using the Hydrologic Engineering Center's Hydrologic Modeling System (HEC-HMS) coupled with the two-dimensional HEC-RAS hydraulic software linked with the

DebrisLib non-Newtonian library. The model simulation adequately predicts the post-wildfire debris flow runout and inundation but has limitations predicting depth and velocity, most likely due to model assumptions of constant sediment concentration and fixed bed.

The final chapter provides a summary and recommendations for future research and development needs. Chapter Five reviews and summarizes the key findings from this research and provides recommendations to address future post-wildfire flood model limitations and assumptions. Future research will aim to continue enhancement of post-wildfire modeling approaches. A selection of future research topics include: dynamic (variable) simulation of deposition and erosion processes, demonstration of applicability and limitations of physics-based numerical models for predicting post-wildfire flooding, enhancement of non-Newtonian hydraulic and sediment transport prediction capabilities, and better understanding and prediction of post-wildfire geomorphic and ecological recovery to improve long-term continuous model approaches.

CHAPTER 2. A MODULAR, NON-NEWTONIAN, MODEL LIBRARY FRAMEWORK (DEBRISLIB) FOR POST-WILDFIRE FLOOD RISK MANAGEMENT

2.1. INTRODUCTION

The number and intensity of large wildfires is a growing concern in the United States. Over the past decade, the National Interagency Fire Centre (NSTC, 2015) reported more large fires in every western state in the arid and semi-arid western region of the country, than any previous decade. Wildfires remove vegetation, reduce organic soil horizons to ash, extirpate microbial communities, and develop hydrophobic soils. These processes all increase water and sediment runoff. Post-wildfire environments can cause a spectrum of hydrologic and sedimentation responses ranging from minor runoff events to catastrophic floods and deadly debris flows. The high sediment concentration exacerbates damages from these events, which have been documented around the world (Rowe et al., 1954; Lane et al., 2006; Shin, 2010; Shakesby, 2011; Moody et al., 2013). In the years following a wildfire, ecotone shifts, gully formation, and channel incision alter the hydrologic system response, resulting in dramatic, and sometimes prolonged changes to downstream systems. Wildfires impact hydrology by removing the rainfall interception canopy, generating ash and charred material, reducing organic binding materials in soils, increasing hydrophobic soils, and modifying the intrinsic and hydraulic properties of soils and sediments (Certini, 2005; Moody et al., 2009; Ebel et al., 2012). Lahars and mine tailing dams also threaten communities and infrastructure around the world and, like post-wildfire flows, these events diverge from classic, Newtonian, shallow-water flow assumptions.

Researchers have developed a range of numerical models to simulate non-Newtonian flows for hazard assessment, flood risk evaluation, and mitigation design (O'Brien et al., 1993; Iverson and Denlinger, 2001; Hungr et al., 2005). These physics-based numerical models simulate

advection with constitutive laws of fluid mechanics in one- and two-dimensions. Savage and Hutter (1989) provided the foundation for predicting non-Newtonian flow using Saint-Venant based shallow-water equations which have been commonly applied for numerical modelling of rapid mass movements over irregular geometry (e.g., Chen and Lee, 2000; Iverson and Denlinger, 2001; Imran et al., 2001; Pudasaini et al., 2005; Naef et al., 2006; Martinez et al., 2007; Pastor et al., 2009; Luna et al., 2012).

There is an increasing need to develop a post-wildfire modelling framework and enhance non-Newtonian numerical modelling capabilities within hydrologic and hydraulic engineering models, for decision making in emergency management and flood risk management operations. However, with the diversity of post-wildfire processes (floods, mudflows, debris flows, etc.) and multiple algorithms available to simulate each process, a formal, modular, library framework that consolidates these algorithms and provides them to multiple hydrodynamic codes will make non-Newtonian implementation more transparent, repeatable, and robust, as demonstrated here. The non-Newtonian algorithm library (DebrisLib) provides a flexible, modular, non-Newtonian, numerical-modelling framework that developers can call from any one-dimensional or two-dimensional shallow-water-based hydraulic and hydrologic model. Consolidating multiple non-Newtonian closures associated with the continuum of geophysical flow processes in a modular library and sharing it between hydrodynamic codes has three main advantages:

1. The library consolidates diverse literature, making a wide suite of algorithms available to each linked model, avoiding duplication of effort.
2. The library makes non-Newtonian modelling more transparent by standardizing algorithm implementation.

3. The library leverages the validation and verification activities of multiple development communities, accelerating the quality control of the code.

This paper documents the numerical library development, enhancements, and linkage architecture necessary for predicting post-wildfire non-Newtonian flood events across different numerical modelling libraries, specifically one- and two-dimensional USACE numerical models. Subsequent papers will look at application of this work to real-world post-wildfire conditions.

2.2. BACKGROUND

Wildfires can significantly shock or perturb semi-arid and arid environments (Pierce et al., 2004; Orem and Pelletier, 2016). Most western U.S. watersheds require decades to recover. These events increase flow and sediment loads, creating immediate and long-term management concerns for federal, state, and local agencies. These management challenges include predicting the post-wildfire flood response of a particular wildfire-precipitation mix. System responses can range from minimal impact, to increased clear water flows, to more destructive ash flows, mud floods, and debris flows. Mudflows, debris flows, and ash flows are unsteady gravity-driven events that involve complex mixtures of sediment, water, and entrained material (i.e., organics, woody debris, unconsolidated substrate). These non-Newtonian flows have high sediment concentrations and can carry large boulders, trees, and uprooted infrastructure (e.g., upstream structures or bridge debris). These flows are commonly modelled using shallow-water equations as either 1) single phase, 2) two-phase, or 3) mixture theory, using non-Newtonian closure approaches and approximations (e.g., Iverson, 1997; Jin and Fread, 1997; Imran et al., 2001). The grain-size distribution, sediment concentration, and flow stress state (as a function of slope) determine which geophysical flow particular wildfire-precipitation events generate.

In addition to the process complexity, modelers face algorithmic diversity challenges. Each of these processes have multiple modeling approaches. Researchers have developed a wide range of algorithms to help apply these rheological and geotechnical modeling libraries to different classifications of geophysical flows. The methods that simulate these post-wildfire flood events are commonly grouped into four main categories:

1) Linear (Bingham 1922) and non-linear viscoplastic models (Jin and Fread 1997; Imran et al. 2001). These approaches use rheological modes as heuristics for cohesive and/or viscous stresses in the fluid and are commonly used to describe the rheology of laminar mud flows.

2) Dispersive-turbulent stress models (O'Brien et al. 1993). This approach adds a turbulent stress term to the dispersive model to describe the inter-particle mechanics within a clay, silt, and organic matrix. This model is commonly applied to sediment mixtures containing cohesive sediment in quantities greater than 10% by volume.

3) Dispersive fluid models (Bagnold 1954 and 1956; Takahashi 1978). The dispersive models use Bagnold's theory to describe the non-linear fluid stress that develops from particle-to-particle interaction between granular, clastic (i.e., silt, sand, or gravel) particles, where the fluid fluctuations keep the particles suspended. This model is commonly applied to sediment-water mixtures containing mostly sand and gravel with lower quantities of fine sediment ($\leq$ 5%–10% by volume).

4) Coulomb-based frictional models (Hungr 1995; Iverson 1997; Iverson and Denlinger 2001). Friction dominated models like Coulomb or Vollemy (Iverson, 1997) take a more geotechnical approach to simulate grain flows that approach library supported conditions, where the internal

mixture stresses are dominated by inter-granular friction. These approaches are often applied to heterogeneous, poorly sorted (well graded), clastic debris flows approaching land-slide classifications. Non-Newtonian flows include several regimes (or flow states) depending on the solid concentration in the fluid and the grain size of the sediment. In general, as concentration increases and grain size coarsens, the fluid-sediment mixture passes through five classifications: 1) Newtonian Flow (clear water or alluvial sediment transport), 2) Hyperconcentrated flow, 3) Mudflow, 4) Grain Flow (coarse-grain hyperconcentrated flow), and 5) Debris (clastic) flow. A taxonomy and conceptual model were developed to simplify the non-Newtonian flow continuum onto a single axis as a function of concentration and grain size distribution shown below in Figure 2.

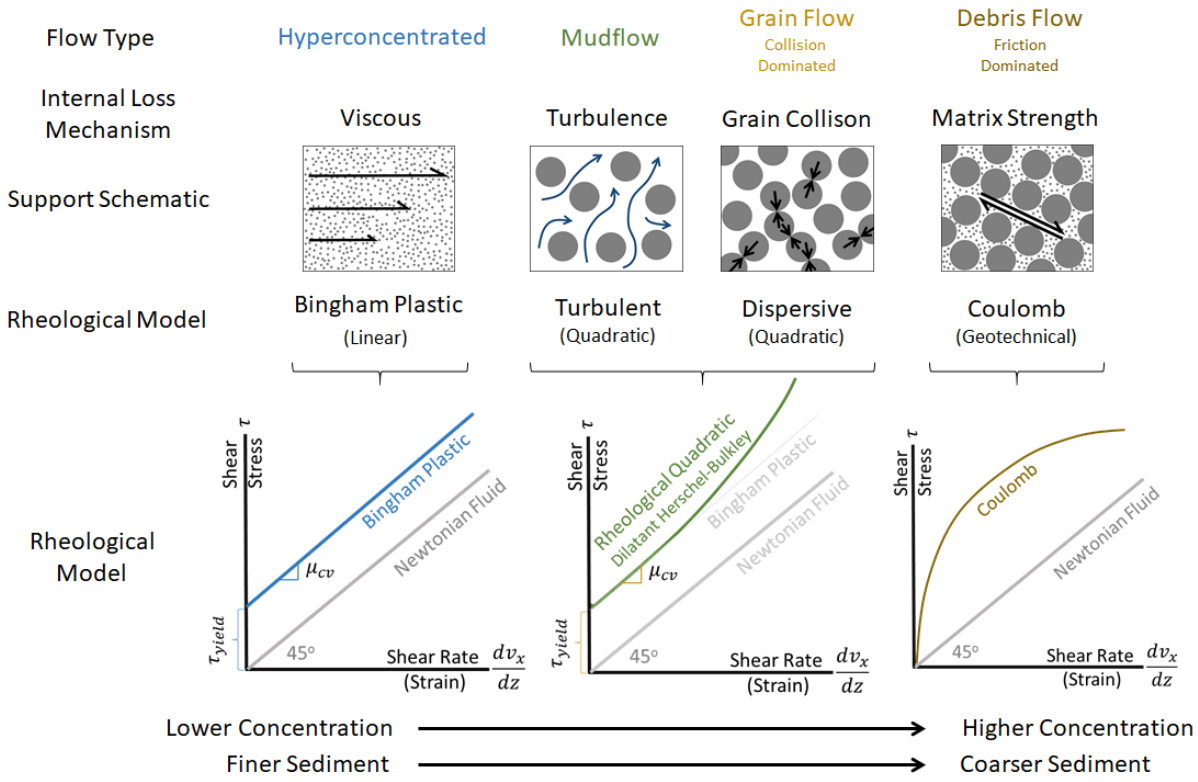

Figure 2. Classification, processes, conceptual model, and rheological model of the four flow conditions in the non-Newtonian model library.

The research team developed a non-Newtonian library (DebrisLib) to simulate the continuum of post-wildfire flood responses along these concentration and grain size gradients, based on rheology and Coulomb theory, to operate independently of the shallow-water parent codes. The non-Newtonian library assembles closure approaches that different shallow-water codes can leverage and determines the flow conditions using non-dimensional threshold parameters. In addition, the library estimates a non-Newtonian drag coefficient (Happel and Brenner, 1965; Julien 2010), addresses hindered settling (Richardson and Zaki, 1954; Baldock et al., 2004; Cuthbertson et al., 2008), computes relative buoyancy terms, and accounts for increased viscosities and mass density (Einstein and Chien, 1955; Dabak and Yucel, 1986). The diversity of the processes and sub-diversity of algorithms for each process makes a shared library approach particularly useful for non-Newtonian model development. Future versions of DebrisLib will address both sediment erosion, transport, and deposition.

Applying non-Newtonian transport in a shallow-water model requires computation of internal losses by adding a slope term to the friction slope (S_f) in the momentum equation and bulking (or increasing) the flow to account for the volume of the solids. The shallow-water friction slope (S_f) accounts for the forces acting against the flow at the fluid boundary (e.g., the channel) while the "mud and debris slope" (S_{MD}) accounts for the internal losses due to the viscosity, turbulence, and/or dispersion within the fluid. The library computes a non-Newtonian shear stress based on the flow classification (e.g., mudflow, debris flow, etc.) and the appropriate rheological approach (i.e., stress-strain model). Then the library integrates the viscous, turbulent, and dispersion shear from the stress-strain model into the momentum equation by converting the shear to a slope and adding this slope to the friction slope. Additionally, because these flows can include between 5%

and 70% solids by volume, a fixed bed model must augment the flow volume to account for the impact of the sediment on the mass and depth of the flow.

2.3. METHODS

2.3.1. Shallow-Water Numerical Models

The shallow-water flow equations solve the continuity and momentum equations simultaneously to compute water stage and velocity. The frictional forces between the fluid and the solid boundary are the primary resisting forces in the standard Newtonian clear-water hydraulic equations. In one dimension, the conservation of mass and momentum are the Saint-Venant equations:

$$\frac{\partial \mathrm{Q}}{\partial \mathrm{x}} + \frac{\partial \mathrm{A}}{\partial \mathrm{t}} - \mathrm{q} = 0 \qquad \text{(Eq. 2.1.)}$$

$$\frac{\partial Q}{\partial x} + \frac{\partial Q\bar{u}}{\partial x} + gA\left(\frac{\partial \eta}{\partial x} + S_f + S_{MD}\right) = 0 \qquad \text{(Eq. 2.2.)}$$

where,

Q = volumetric flow discharge (m^3/s)

x = downstream distance in channel (m)

t = time (s)

A = cross sectional area of channel (m^2)

q = lateral inflow or outflow (m^2/s)

η = water surface elevation (m)

S_f = Newtonian friction slope (m/m).

S_{MD} = Mud and debris friction slope (m/m).

In two dimensions the shallow-water equations vertically integrate the mass and momentum equations under the assumptions of incompressible flow and hydrostatic pressure. Assuming negligible free surface shear and pressure variations at the free surface, the two-dimensional shallow-water equations are:

$$\frac{\partial Q}{\partial t}+\frac{\partial F_x}{\partial x}+\frac{\partial F_y}{\partial y}+H=0 \qquad \text{(Eq. 2.3.)}$$

$$Q=\begin{Bmatrix} h \\ uh \\ vh \end{Bmatrix} \qquad \text{(Eq. 2.4.)}$$

$$F_x=\begin{Bmatrix} uh \\ u^2h+\frac{1}{2}gh^2-h\frac{\sigma_{xx}}{\rho_m} \\ uvh-h\frac{\sigma_{yx}}{\rho_m} \end{Bmatrix} \qquad \text{(Eq. 2.5.)}$$

$$F_y=\begin{Bmatrix} vh \\ uvh-h\frac{\sigma_{xy}}{\rho} \\ vh+\frac{1}{2}gh^2-h\frac{\sigma_{yy}}{\rho} \end{Bmatrix} \qquad \text{(Eq. 2.6.)}$$

$$H=\begin{Bmatrix} 0 \\ gh\frac{\partial z_b}{\partial x}+gh\frac{n^2u\sqrt{u^2+v^2}}{h^{\frac{4}{3}}}+ghS_{MDx} \\ gh\frac{\partial z_b}{\partial y}+gh\frac{n^2v\sqrt{u^2+v^2}}{h^{\frac{4}{3}}}+ghS_{MDy} \end{Bmatrix} \qquad \text{(Eq. 2.7.)}$$

where

ρ_m = mixture density (kg/m^3)

u = flow velocity in the x direction (m/s)

v = flow velocity in y direction (m/s)

h = flow depth (m)

σ_{ij} = Reynolds stresses due to turbulence (Pa)

S_{MDx} = Mud and debris slope in the x direction (m/m)

S_{MDy} = Mud and debris slope in the x direction (m/m)

Where the first subscript indicates the direction and the second indicates the face on which the stress acts.

g = gravitational acceleration (m/s^2)

z_b = bottom elevation (m)

n = Manning's roughness coefficient

The Reynolds stresses are determined using the Boussinesq approach to the gradient in the mean current:

$$\sigma_{xx} = 2\rho_m \nu \frac{\partial u}{\partial x} \qquad \text{(Eq. 2.8.)}$$

$$\sigma_{yy} = 2\rho_m \nu \frac{\partial v}{\partial y} \qquad \text{(Eq. 2.9.)}$$

$$\sigma_{xy} = \sigma_{yx} = \rho_m \nu \left(\frac{\partial u}{\partial y} + \frac{\partial v}{\partial x}\right) \qquad \text{(Eq. 2.10.)}$$

The depth-averaged Shallow Water Equations model in HEC-RAS solves volume and momentum conservation equations and includes temporal and spatial accelerations as well as horizontal mixing while the diffusive wave equation model ignores these processes but is

therefore simpler and more computationally efficient. The 2D volume conservation of the water-solid mixture is given by:

$$\frac{\partial \eta}{\partial t} + \frac{\partial (hu)}{\partial x} + \frac{\partial (hv)}{\partial y} = q \qquad \text{(Eq. 2.11.)}$$

where η is the flow surface elevation, t is time, h is the water depth, V is the velocity vector, and q is a source or sink term, to account for external and internal fluxes. The depth-averaged momentum conservation equations may be written as (Hergarten and Robl, 2015):

$$\frac{\partial u}{\partial t} + u\frac{\partial u}{\partial x} + v\frac{\partial u}{\partial y} = -g\cos^2\varphi \frac{\partial \eta}{\partial x} + \frac{1}{h}\frac{\partial}{\partial x}\left(v_t h \frac{\partial u}{\partial x}\right) + \frac{1}{h}\frac{\partial}{\partial y}\left(v_t h \frac{\partial u}{\partial y}\right) - \frac{\tau_x}{\rho_m R}\frac{\cos\psi}{\cos\varphi} \qquad \text{(Eq. 2.12.)}$$

$$\frac{\partial v}{\partial t} + u\frac{\partial v}{\partial x} + v\frac{\partial v}{\partial y} = -g\cos^2\varphi \frac{\partial \eta}{\partial y} + \frac{1}{h}\frac{\partial}{\partial x}\left(v_t h \frac{\partial v}{\partial x}\right) + \frac{1}{h}\frac{\partial}{\partial y}\left(v_t h \frac{\partial v}{\partial y}\right) - \frac{\tau_y}{\rho_m R}\frac{\cos\psi}{\cos\varphi} \qquad \text{(Eq. 2.13.)}$$

where:

g = the gravitational acceleration (m/s^2)

v_t = turbulent eddy viscosity (m^2/s)

$\tau = (\tau_x, \tau_y)$ is the total basal stress (Pa)

ρ_m = the water-solid mixture density

R = the hydraulic radius (m)

φ = the water surface slope (m/m)

ψ = the inclination angle of the current velocity direction (deg).

In the above equations, the second term on the right-hand-side represents the horizontal mixing due to turbulence and also in the case of a debris flow, horizontal mixing due to particle collisions. Utilizing the conservative form of the mixing terms is essential for accurate momentum conservation. The bottom friction coefficient is computed utilizing the Manning's roughness coefficient as

$$\tau = \tau_{\text{turbulent}} + \tau_{\text{MD}} \qquad \text{(Eq. 2.14.)}$$

where

$\tau_{turbulent}$ = the turbulent stress

τ_{MD} = the mud and debris stress

which includes all non-Newtonian stresses. The turbulence bottom shear stress is computed as a function of the Manning's roughness coefficient. The mud and debris stress are described in detail in the section "Rheological Models". It is noted that when the non-Newtonian stress is equal to zero and the cosine functions (slope corrections) are removed, the above 2D shallow-water equations reduce to the clear-water equations utilized in HEC-RAS.

2.3.2. Non-Newtonian Shallow-Water Closure

Mud and debris flows generate additional resisting forces. Increasing the solid content increases the viscosity of non-Newtonian flows, generating internal resisting forces within the fluid. At higher concentrations, particularly with coarse particles, particle collision and friction introduce additional internal resisting forces. Most of the theoretical and numerical modifications involve integrating the new internal fluid forces in the momentum equation. The depth-averaged equations can be adapted for non-Newtonian simulations by adding an additional loss slope term (S_{MD}) to the classic friction slope term (S_f) in the conservation of momentum equation.

DebrisLib computes this Mud and Debris slope that the hydrodynamic models add to the momentum equation by computing internal shear stresses that the different non-Newtonian processes generate based on rheology or Coulomb models (see Figure 1). The library then converts the internal, rheological shear (τ_{MD}) from the hypothesized stress-strain characteristics into a fluid loss Mud and Debris slope (S_{MD}):

$$S_{MD} = \frac{\tau_{MD}}{\rho_m g R} \qquad \text{(Eq. 2.15.)}$$

where

ρ_m = the sediment-fluid mixture density (kg/m^3)

R = the hydraulic radius (m)

The O'Brien et al. (1993) quadratic, rheological model combines the four stress components of non-Newtonian sediment mixtures: (1) cohesion between particles, (2) internal friction between fluid and sediment particles, (3) turbulence, and (4) inertial impact between particles. The quadratic model separates the stress-strain relationships into these four, additive components, such that the shear stress is:

$$\tau_{MD} = \tau_{yield} + \tau_{viscous} + \tau_{turbulent} + \tau_{dispersive} \qquad \text{(Eq. 2.16.)}$$

where

τ_{MD} = the total mud-and-debris shear stress (Pa)

τ_{yield} = yield stress (Pa)

$\tau_{viscous}$ = viscous shear stress (Pa)

$\tau_{turbulent}$ = turbulent shear stress (Pa) (similar to Manning's roughness in O'Brien et al., 1993)

$\tau_{dispersive}$ = dispersive shear stress (Pa)

O'Brien et al. (1993) define these terms, yielding a quadratic model based on the strain (dv_x/dz):

$$\tau_{MD} = \tau_y + \mu_m \left(\frac{dv_x}{dz}\right) + \rho_m l_m^2 \left(\frac{dv_x}{dz}\right)^2 + c_{Bd}\rho_s \left(\left(\frac{C_*}{C_v}\right)^{1/3} - 1\right)^{-2} d_s^2 \left(\frac{dv_x}{dz}\right)^2 \qquad \text{(Eq. 2.17.)}$$

where,

dv_x/dz = the shear rate (1/s) computed as a function of depth averaged velocity and flow depth

μ_m = mixture dynamic viscosity (Pa s)

ρ_m = sediment mixture mass density (kg/m^3)

l_m = mixing length (m)

c_{Bd} = Bagnold impact empirical coefficient ($c_{Bd} \cong 0.01$)

ρ_s = sediment particle density (kg/m^3)

C_*= maximum volumetric sediment concentration (-)

C_v = volumetric sediment concentration (-)

d_s = sediment grain size (m)

Takahashi (1980) identified experimentally that the Bagnold impact coefficient (c_{Bd}) ranges between 0.35 and 0.5 and that is significantly larger than the value recommended from Bagnold (1954 and1956). Iverson (1997) defined the strain (or shear rate) $(3\bar{u}/h)$ is based on a vertical integration of a parabolic velocity profile or $(2\bar{u}/h)$ for linear velocity profile conditions, where,

$\bar{u}$ = depth averaged velocity (m/s)

h = flow depth (m).

Therefore, the quadratic model requires two new terms: the mixture density and the Prandtl mixing length. The equation for the Prandtl mixing length is defined as

$$\mathrm{l_m} = \mathrm{kz} \qquad (\mathrm{Eq.\ 2.18.})$$

Where, k = the Von Karmen coefficient ($\cong 0.41$) and z = the proportional distance from the boundary (bed).

This quadratic model combines linear and non-linear rheological modes to compute internal shear. Rheological models do not perform as well as the mixtures get more clastic (i.e., high concentrations of coarse particles). DebrisLib simulates clastic debris flows with a Coulomb approximation based on the Johnson and Rodine (1984) Coulomb viscous model (Naef et al., 2006). This approach replaces the Bingham yield strength (τ_y) a geotechnical, Coulomb yield stress defined as,

$$\tau_{yc} = \rho_m g h \cos\alpha \tan\varphi \qquad \text{(Eq. 2.19.)}$$

where,

τ_{yc} = Coulomb yield stress (Pa)

α = bed slope angle (°)

φ = Coulomb friction angle (°) with typically ranges between 30° and 40° (Iverson, 1997; McArdell et al., 2007).

The Coulomb friction angle is a function of the individual grain friction angle and the packing geometry of the particles along the failure plane.

2.3.3. Numerical Model Discretization

The solution of Equations 2.1 through 2.19 can be achieved through discretization in time and space. Temporal discretization of the equations is achieved through explicit or implicit solution schemes. Explicit schemes rely on the solutions from the previous time steps to obtain the new time step solution, and implicit schemes rely on the previous, present, and future solutions to obtain the new time step solution. Numerical techniques for the spatial discretization include finite-difference method (FDM), finite-volume method (FVM), finite-element method (FEM), and meshless methods. In this manuscript we used the FEM and the FVM for the spatial

discretization of the afore-mentioned equations. We used the USACE 1D and 2D HEC-RAS and 2D AdH models to test the robustness of the developed techniques. HEC-RAS solves the diffusive wave equation (DWE) and the depth-averaged shallow-water equations (SWE). The DWE is solved using an implicit FVM. The SWE are solved with a combination of FDM and FVM and a semi-implicit time stepping scheme. Water volume conservation is ensured by a finite-volume discretization of the continuity equation. The momentum equation is discretized semi-implicitly using the FDM. HEC-RAS uses a subgrid modelling approach which describes the high-resolution subgrid terrain using hydraulic property tables allowing for larger computational cells and time steps while still maintaining accuracy. The subgrid approach leads to a mildly nonlinear system of equations which is solved using a Newton-type iteration algorithm (HEC 2016). HEC-RAS solves the FMSWE and the DWE using a combination of implicit finite-difference and finite-volume methods on an unstructured polygonal mesh.

AdH suite is a collection of solvers for the unsaturated Richard's equations, Reynolds Averaged Navier Stokes Equations (RANS), full momentum shallow-water equations (FMSWE), and the DWE. The FMSWE and the DWE can be meshed in space using the Cartesian or the spherical coordinate system. AdH uses the FEM method with implicit time stepping to solve the equations of motion and conservation of mass. AdH has been widely discussed in engineering literature and the interested reader is referred to Savant et al. (2019), Savant et al. (2018), Trahan et al. (2018), Savant and McAlpin (2014), Savant and Berger (2012), and Savant et al. (2011) for additional details on the AdH model.

2.3.4. Validation Datasets

The validation process involved simulation of multiple flume experiments selected to represent the continuum of non-Newtonian flow behavior under both steady and unsteady conditions. This

includes the Jeyepalan (1981) and Hungr (1995) unsteady dam break analytical solutions, Haldenwang (2003) steady-state flume experiments, and the large-scale U.S. Geological Survey (USGS) flume experiments of high-concentration debris flow conditions from Iverson et al. (1992 and 2010). Initial verification of DebrisLib was conducted using the 1D analytical solutions from an idealized 30-meter-high tailings dam subjected to instant liquefaction failure from Jeyapalan (1981) and Hungr (1995). The primary validation variables included failure runout distance, velocity, depth, and cessation of flow. The initial validation flume experiments are from Haldenwang et al. (2006) who conducted flume experiments using kaolinite, bentonite, and solution of carboxymethyl cellulose polymer with various concentration ranging from 1% to 10% by volume. The experiments were conducted in two tilting flumes, one 10-m long and 300-mm wide and the other flume 5-m long and 75-mm wide. Slope varied ranging from 1º to 5º. In this research only the results from the 10-m flume are presented. The final experiments utilized were the USGS debris flow flume at H.J. Andrews Experimental Forest, Oregon, United States (Iverson et al., 1992; Iverson 1992; Iverson et al., 2010). The USGS conducted large-scale debris flow experiments between 1994 and 2004. The USGS flume experiments consisted of rapid releases of saturated, nonuniformly sized sediment mixtures (Iverson et al., 2010). Experiments where conducted in a 95-m-long, 2-m-wide flume with a maximum slope of approximate 31º for both fixed- and mobile-bed conditions for a wide range of sediment gradations and concentrations. The headgate is positioned at 12.5 m downslope. This section leads to a reach in which the slope follows a catenary curve descending 2.2 m vertically before reaching an outlet to a runout surface with a gentle slope of 2.4º extending 107.5 m. The rough concrete tiles are positioned between 6 to 79 m from the release gate. The height of debris behind the headgate was 1.9 m. Simulations presented here were conducted for fixed-bed experiments using debris

mixtures of about 56% gravel, 37% sand, and 7% mud particles (Iverson et al., 2010). The HEC-RAS grid for the USGS flume experiment has a constant grid resolution of 0.15 and 0.2 in the downslope and transverse directions respectively with a total of approximately 13,350 cells.

2.4. RESULTS

The model library and the linkage architecture were evaluated by simulating two non-Newtonian validation data sets by calling the library from two different hydrodynamic codes. To evaluate the model library a selection of flume experiments was used to demonstrate the library's flexibility using both small- and large-scale flows of various grain size distributions and sediment concentrations. These flume experiments were selected to demonstrate the flexibility of the model library and its linkage architecture with USACE shallow-water models. The data sets simulated include: equilibrium, hyperconcentrated flow (volumetric concentration, Cv=10%) from Haldenwang et al. (2006) experiments and an analytical, unsteady non-Newtonian dam break with a higher concentration (Cv=55%) from Jeyapalan 1981 and Hungr (1995) running out until flow stops or yields. Input conditions and calibration data for Hungr (1995), Haldenwang et al. (2006), and Iverson et al. (2010) experiments are provided in Table 1.

Table 1. Input parameters for modelled experiments.

Variables	**Hungr (1995)**	**Haldenwang et al. (2006)**	**Iverson et al. (2010) USGS Flume**
Impoundment Height (m)	30	—	1.9
Volumetric Concentration (%)	55	10	61.2
Mixture Density (kg/m^3)	2500	1165	2010
τ_y (Pa)	1500	21.3	—
d_s (mm)	0.025	0.02-0.04	0.0625-5.0
O'Brien Power Coefficient	0.75	0.05	
O'Brien Yield Coefficient	6	9	

(table cont'd)

Variables	Hungr (1995)	Haldenwang et al. (2006)	Iverson et al. (2010) USGS Flume
O'Brien Viscosity Coefficient	9.1	8	
Hershel Bulkley Coefficient (k) ($Pa.s^n$)	—	0.524	
Hershel Bulkley Power (n)	—	0.468	
Yield Strength (Pa)	1496.4	23.84	
Dynamic Viscosity (Pa s)	101.2	0.00316	
Domain Length (m)	2000	10	107.5
Domain Width (m)	—	0.015	2

*Coefficients from O'Brien et al. (1993) yield strength and dynamic viscosity.

It is important to note that this research only presents our general findings regarding USACE hydrology and hydraulic modelling capabilities. Subsequent research and publications will focus on the additional details for the provided flume experiments. The 2D HEC-RAS and AdH results for the Jeyapalan 1981 and Hungr (1995) dam breach simulations are included in Figure **3** (left and right respectively) representing dynamic unsteady conditions following an impoundment failure. The initial profile represents the 30-m-high pre-dam break conditions, and the final profile is the analytical solution for the failure runout profile when the flow ceases. This analytical dam removal solution allows for computation of the "runout length," which is the distance required for this high-energy mass flow to come to rest (i.e., the shear stress drops below the yield strength). Both numerical simulations compute runout lengths very similar to Hungr's (1995) result and have similar final depth profiles. Both HEC-RAS and AdH sufficiently replicated the impoundment failure to include unsteady runout, flow depth and velocity. These results were consistent with other publications based on this analytical solution (e.g., Naef et al., 2005). Simulations were conducted using Bingham, Herschel-Bulkley, and

O’Brien quadratic models with only Bingham rheology conditions presented, with all cases exhibiting similar flow behavior and results.

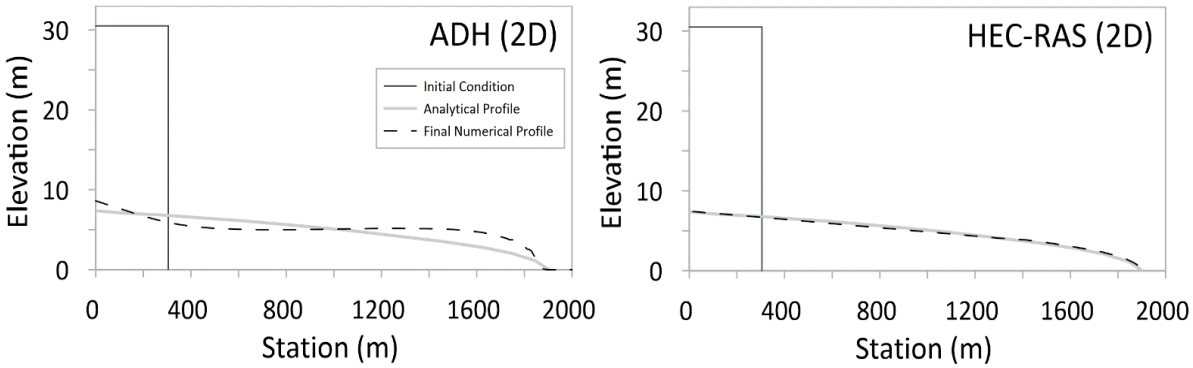

Figure 3. Simulation of Hungr (1995) dam breach experiments with two-dimensional Adaptive Hydraulics.

The results from the Haldenwang et al. (2006) simulations are included in Figure 4. HEC-RAS + DebrisLib using the 1D, finite-difference and 2D AdH finite-element, unsteady flow (with a constant flow boundary condition) modelling frameworks to simulate stages associated with multiple experimental flows with four different rheological assumptions. In both cases the non-Newtonian simulations compute fluid stage better than clear water flow. As shown, overall agreement is good between flume experiments and model simulations, and agreement is reasonable across all rheology closures presented to include Bingham, Herschel-Bulkley, and O’Brien quadratic models plotted with the Newtonian shallow-water results. Bingham and O’Brien provide the most accurate representation of the flow and depths for the 5-degree flume conditions. This is consistent for both HEC-RAS and AdH simulations. The differences between HEC-RAS and AdH results are likely due to a range of factors, to include how each model accounts for initial conditions, model discretization, grid size, and time step size. All rheology closure models simulated under predict depth-flow curve at flow ranges smaller than approximately 7.5 L/s, likely a result of several factors, to include the strain rate approximation

of $^{3u}/_{h}$, change in velocity profile, potential sediment deposition, or a combination. This will be investigated more thoroughly in subsequent research. Interestingly all models did better at predicting transitional and turbulent conditions versus laminar (as shown with the red line in Figure 4). Only one previous study was found that used the Haldenwang data set for comparison with a shallow-water model (Perez, 2017), but our results are consistent with those findings. Additional model research is ongoing using this dataset aimed at better quantifying turbulent behavior at lower sediment concentrations analogous to hyperconcentrated flows. This will also help better understand the deviations between model and flume results for flow conditions less that about 5 L/s.

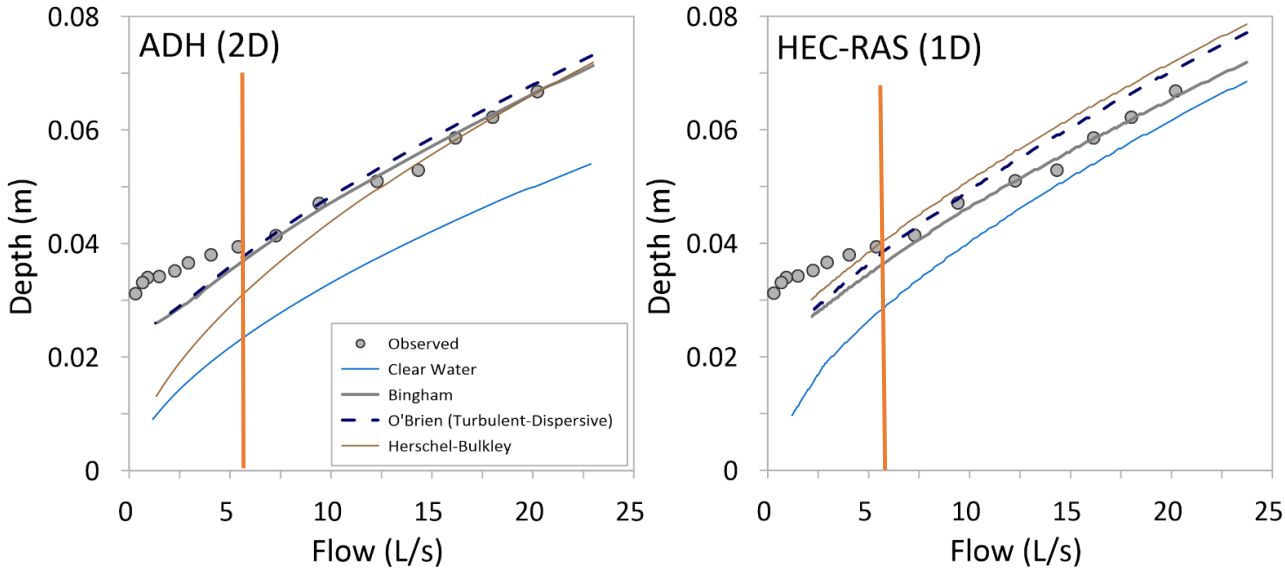

Figure 4. Simulation of Haldenwang et al. (2010) flume experiment with one-dimensional HEC-RAS and two-dimensional AdH numerical model. With red line indicating transition from turbulent to laminar flow conditions.

AdH and HEC-RAS are compared against the USGS flume experiment with a representative experiment with a mixture of sand, gravel, and mud (silts and clays) and a section of bumpy concrete tiles. The comparison of AdH and HEC-RAS water levels compared to the

measurements from one of the USGS experiments is presented in Figure 5. Both AdH and HEC-RAS water surface time series compared reasonably well with depth measurements. Differences in AdH and HEC-RAS results are due to differences in the model formulation and numerical assumptions and solution methods. This demonstrates that the optimal rheological parameters will likely be different for different models. As shown in Figure **5**, AdH more closely replicated the USGS flume results compared to the HEC-RAS results due to the adaptive time step and the more advance solution procedure. Both models tend to do better at the upstream locations specifically, at x = 2 m and x = 32 m. Model results continue to deviate from flume conditions slightly for x = 66 m and x = 90 m with more pronounced deviation seen in the HEC-RAS results. These differences are the result of the flume slope being approximately 31 degrees, which violates the shallow-water assumptions of most depth-averaged models, including these. Surprisingly they still perform reasonably well, considering this limitation.

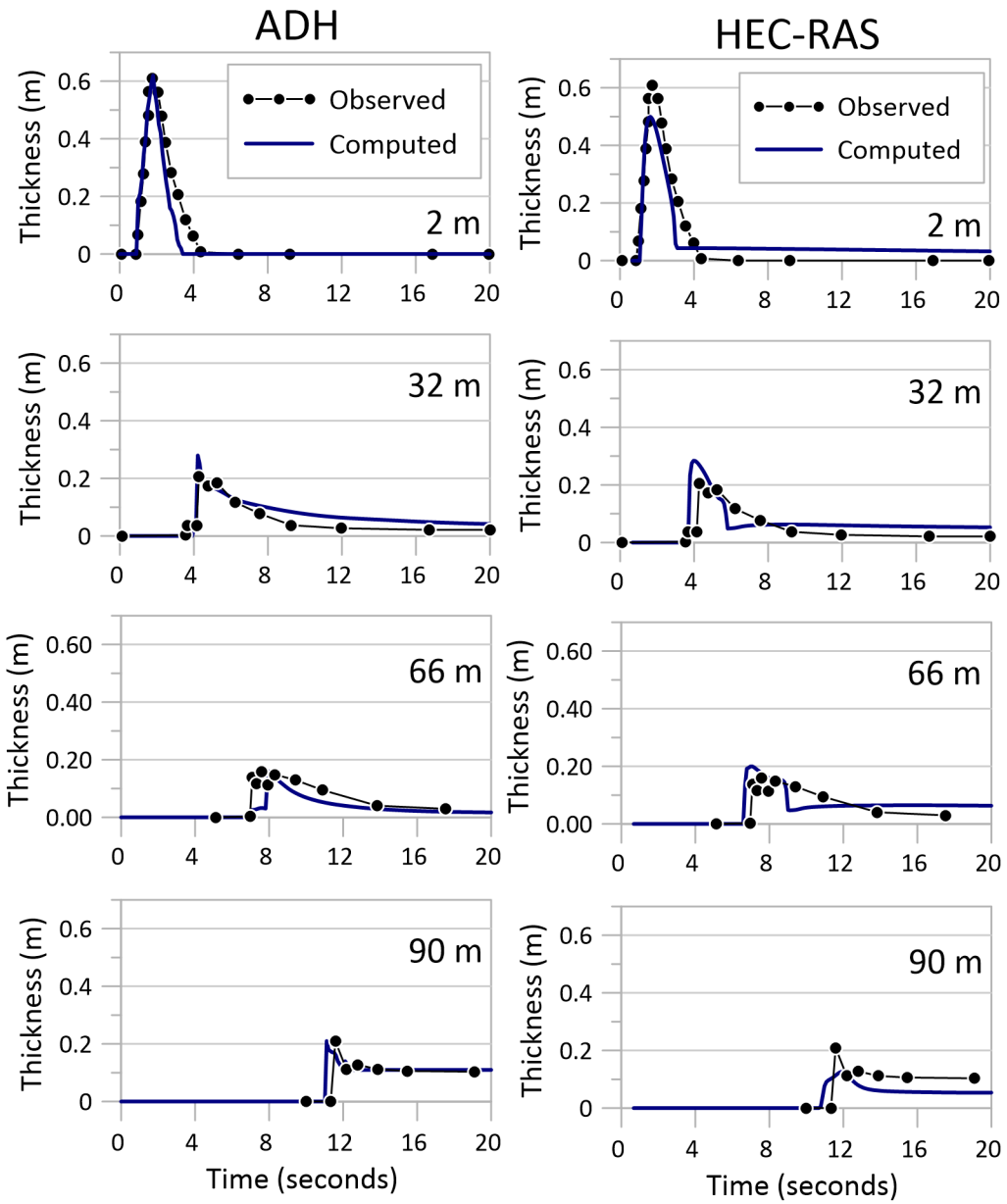

Figure 5. Simulation of USGS flume experiments (Iverson et al., 2010) with two-dimensional HEC-RAS and two-dimensional AdH numerical models. With the 2m, 32m, 66m, and 90m representing measurement location downstream from gate.

2.5. DISCUSSION

The post-wildfire non-Newtonian model library DebrisLib expands upon the quadratic model (O'Brien et al., 1993) to predict a range of post-wildfire sedimentation behavior across multiple numerical model platforms. The flexible non-Newtonian library allows for prediction of a range of post-wildfire flood conditions demonstrated using a two shallow-water numerical models. We

introduce a modification to existing non-Newtonian taxonomy and classification describing common non-Newtonian post-wildfire flows and demonstrate using both 1D and 2D shallow-water numerical models for a range of non-Newtonian flow conditions. To date, existing non-Newtonian models predict a limited range of flow conditions within a single modelling platform, thus multiple models must be merged together to address the full range of flow conditions. The process and approach diversity of the non-Newtonian literature in particular make a modular computation library-based framework advantageous by consolidating the algorithms for each process. With a few common variables like depth, velocity, mixture density, and slope, the model library can be linked with most existing shallow-water Newtonian numerical models, regardless of dimension, library, or solution method, to predict non-Newtonian flows. Currently the model library is under development with planned released scheduled soon. Simulating a range of flow conditions across multiple non-Newtonian transport models will increase access to post-wildfire modelling capabilities and reduce uncertainty associated with comparisons from multiple independent model approaches. Furthermore, this research constitutes the first non-Newtonian simulations using USACE shallow-water models.

The flexibility will allow broader access to the non-Newtonian modelling capabilities for practitioners, managers, and researchers to improve understanding of the model limitations and operational modelling for post-wildfire emergency management and flood risk management. During development of the model library, the team identified some key disadvantages and advantages associate with library-based frameworks in research and development. An overview of the advantages and challenges associated with development of a flexible library-based model framework are provided below in Table 2.

Table 2. Advantages and challenges associated with library-based frameworks.

Advantages	Disadvantages/Challenges
• Standardization and Transparency • Leverages contributions • Improves debugging and development • Encourages scientific communication	• Requires continuous communication • Research and development can take longer • Requires team commitment • Focuses on physical processes violating most empirical prediction approaches

More specifically, the disadvantages and challenges identified are: 1) Modifications and changes during research and development require continuous communication between developers; 2) Because these changes and modifications require constant coordination, research and development takes longer; 3) Requires commitment from all collaborators to ensure success; and 4) Focuses on physical process may violate most empirical prediction approaches. Advantages include: 1) Standardization of computation approaches and closure between model frameworks; 2) Results in transparency in approach and assumptions; 3) Leverages contributions from multiple researchers and teams, minimizing duplication; 4) Improves debugging and development production by expanding QA/QC capabilities; and 5) Encourages scientific communication between research teams by requiring explicit negotiations when addressing challenges and setbacks during development.

2.6. CONCLUSION

High-intensity wildfires remove vegetation, alter soils, modify subsurface root structures, purge organic soil, and create widespread hydrophobic soils. This increases runoff, erosion, and sediment transport, which results in destructive flooding. Wildfire effects can generate gravity-

driven surface runoff and erosion events that involve complex mixtures of water, ash, sediment, and entrained debris (i.e., destroyed upstream infrastructure, woody debris, and very large sediment clasts). Several other geophysical flows, including lahars and mine tailing dam failures have similar non-Newtonian dynamics and require these closures to model them effectively. How can hydrologic and hydraulic models improve existing non-Newtonian numerical modeling capabilities? The work presented here consolidates the state-of-the-practice in a modular, non-Newtonian sediment transport library. Then, the work demonstrates easy connection of the library to multiple modelling platforms with different dimensionality, interfaces, and mesh requirements, and accurately predict analogues physics common in post-wildfire non-Newtonian flow conditions. This modular library improves and enhances prediction capabilities to assist with planning, management, and mitigation in post-wildfire environments using practical science-based approaches and smart integrated numerical approaches.

CHAPTER 3. EVALUATION OF NON-NEWTONIAN TURBULENCE WITHIN A 2D SHALLOW-WATER NUMERICAL MODEL

3.1. INTRODUCTION

In arid and semi-arid mountainous regions, destructive non-Newtonian flows are a typical response from the physical and hydrologic effects driven by wildfires (Cannon and Reneau, 2000; Cannon and Gartner, 2005; Shakesby and Doerr, 2006; Burns et al., 2015). Non-Newtonian flow originating in recently burned watersheds can greatly contribute to the overall damage and economic losses annually produced by wildfires (Parise and Cannon, 2012). These non-Newtonian flows can range from low sediment concentrated hyperconcentrated "ash" flows to higher concentrated mud flows and debris flows posing challenges for post-wildfire emergency and flood risk management. Burn et al. (2015) identify two conditions for initiation of runoff related non-Newtonian debris flows; sufficient water runoff and abundant fine grain soils and sediments, both of which are in abundance after intense wildfires. Following a wildfire, runoff can significantly increase through loss of vegetation precipitation inception canopy, development of soil hydrophobicity, and decreased surface runoff roughness. In addition, sufficient amounts of fine soils and sediment are produced through heat induced disaggregation of soils and sediments and production of burned organic ash. With the potential for variability in post-wildfire flow behavior throughout the watershed and along the flow path, it becomes important to quantify at which point turbulence is the dominant form of physical dissipation within the non-Newtonian flow.

The purpose of this research is to evaluate the non-Newtonian Bingham, HB, and O'Brien et al. (1993) quadratic rheology models for predicting turbulent homogeneous non-Newtonian flow conditions. This is done using the two-dimensional HEC-RAS and AdH numerical models that

are linked to DebrisLib, simulation of Haldenwang (2003) flume experiments, and model validation. The research aim is to improve operational (engineering) numerical modeling capabilities for predicting turbulent flow behavior commonly observed during post-wildfire flood events. The rheology models provide the foundation for evaluation and comparison of various turbulent approaches modified from existing non-Newtonian literature and Newtonian. Post-wildfire floods, especially with high ash content, have been documented to behave as turbulent flow. This behavior has been observed over a wide range of physical conditions, sediment concentrations, and fire specifics (Moody et al., 2013). Thus requiring a detailed study on the accurary of the open channel non-Newtonian turbulent modeling within widespread engineering (operational-based) software platforms. The research questions of interest are 1) How effective are current state-of-practice rheology models at non-Newtonian turbulent flow conditions within a shallow-water numerical model and 2) Can existing state-of-the-knowledge approaches be used to distinguish between turbulent and non-turbulent non-Newtonian conditions?

The objectives of this research are as follows;

1) Development of a numerical model representing Haldenwang (2003) experiments selected to represent a range of non-Newtonian turbulent behavior;

2) Calibrate and then validate to flume experiments using the multidimensional model to evaluate the quadratic model turbulent approach using the 2D adaptive hydraulics model of formulation of turbulent flow; and

3) Development of a conceptual model to identify the transition between turbulent and non-turbulent conditions.

Several post-wildfire effects result in abundant water: loss of inception canopy, development of hydrophobic soils, and decreasing surface roughness. Fine sediments have two potential sources

in burned landscapes: particle disaggregation from high temps and development of organic ash (Cannon and Renew, 2000). Following a wildfire, vast quantities of ash have been documented layering across watersheds, with substantial amounts of ash deposits following post-wildfire debris flows (Cannon, 2001; Cannon et. al., 2001a; Meyer and Wells, 1997). In contrast to non-Newtonian flows that generate through the fluidization of falling landslides (e.g., Iverson, 1997; Gabet and Mudd, 2006), debris flows and recently burned watersheds initiate primarily by progressive bulking of surface runoff.

Findings from Burns 2007 and Burns and Gabet (2015) indicate that the rheology of ash slurries deviates from the mineral counterparts. They determined high-concentration ash slurries were strongly shear-thinning compared to slurries composed of similar size silt particles. This increased pseudo-plastic behavior suggests that at low shear rates, ash particles, or structures of ash particles, hinder each other to a greater degree than mineral particles (Major and Pierson, 1992). Alternatively, the aggregates are likely breaking apart at higher shear rates with studies documenting a 50% decrease in median diameter of ash particles forcefully stirred in water, suggesting that ash aggregates can break apart when sheared (Gabet and Bookter, 2001).

Applying non-Newtonian numerical models requires several potential modifications to the shallow-water equations solving the continuity of momentum and mass. The modifications are model dependent but the most common are: modifying the friction slope in the momentum equations; bulking of the flow to account for additional solid volume; and modifying viscosity. Non-Newtonian turbulent flow in channels has been extensively investigated, but the behavior of turbulence in non-Newtonian flows has been mostly limited to pipe flow conditions (Mooney, 1931; Gover, 1972; Wilson, and Thomas, 1985 and 2006). Contrary to pipe flow, very limited attempts have been made to investigate non-Newtonian turbulence in open channel conditions.

Niak (1983) investigated the flow in fluids under turbulent flow conditions using turbulent Newtonian open-channel flow models. More recently Haldenwang (2003) conducted extensive flume experiments for turbulent non-Newtonian conditions and developed models for predicting the onset of turbulent flow conditions derived from pipe flow theory.

3.2. METHODOLOGY

3.2.1. Rheological Non-Newtonian Modeling

Within most hydraulic models, the shallow-water equations are obtained by vertically integrating the mass and momentum equations under the assumptions of incompressible flow and hydrostatic pressure. Assuming negligible free surface shear and pressure variations at the free surface, the two-dimensional shallow-water equations are written as

$$\frac{\partial Q}{\partial t} + \frac{\partial F_x}{\partial x} + \frac{\partial F_y}{\partial y} + H = 0 \qquad \text{(Eq. 3.1.)}$$

$$Q = \begin{Bmatrix} h \\ uh \\ vh \end{Bmatrix} \qquad \text{(Eq. 3.2.)}$$

$$F_x = \begin{Bmatrix} uh \\ u^2h + \frac{1}{2}gh^2 - h\frac{\sigma_{xx}}{\rho} \\ uvh - h\frac{\sigma_{yx}}{\rho} \end{Bmatrix} \qquad \text{(Eq. 3.3.)}$$

$$F_y = \begin{Bmatrix} vh \\ uvh - h\frac{\sigma_{xy}}{\rho} \\ vh + \frac{1}{2}gh^2 - h\frac{\sigma_{yy}}{\rho} \end{Bmatrix} \qquad \text{(Eq. 3.4.)}$$

$$H = \begin{Bmatrix} 0 \\ gh\frac{\partial z_b}{\partial x} + gh\frac{n^2 u\sqrt{u^2+v^2}}{h^{\frac{4}{3}}} + gh\frac{\tau_{mdx}}{\rho_m} \\ gh\frac{\partial z_b}{\partial y} + gh\frac{n^2 v\sqrt{u^2+v^2}}{h^{\frac{4}{3}}} + gh\frac{\tau_{mdy}}{\rho_m} \end{Bmatrix} \quad \text{(Eq. 3.5.)}$$

where,

ρ = fluid density (kg/m^3)

u = flow velocity in the x direction (m/s)

v = flow velocity in y direction (m/s)

h = flow depth (m)

σ_{ij} = Reynolds stresses due to turbulence (Where the first subscript indicates the direction and the second indicates the face on which the stress acts)

g = gravitational acceleration (m/s^2)

z_b = bottom elevation (m)

n = Manning's roughness coefficient.

The Reynolds stresses are determined using the Boussinesq approach to the gradient in the mean current.

$$\sigma_{xx} = 2\rho_m \nu_m \frac{\partial u}{\partial x} \quad \text{(Eq. 3.6.)}$$

$$\sigma_{yy} = 2\rho_m \nu_m \frac{\partial v}{\partial y} \quad \text{(Eq. 3.7.)}$$

$$\sigma_{xy} = \sigma_{yx} = \rho_m \nu_m \left(\frac{\partial u}{\partial y} + \frac{\partial v}{\partial x}\right) \quad \text{(Eq. 3.8.)}$$

Two non-Newtonian closure approaches will be tested using the numerical models: addition of non-Newtonian friction slope and modification of the Reynolds stress equations. The Reynolds stresses will be modified to include non-Newtonian viscosity and mixture mass density, as defined in Equations 3.6 through 3.8.

3.2.2. Computing Internal Losses with Rheological Models

The O'Brien et al. (1993) quadratic model combines four stress components important in non-Newtonian sediment-water mixtures: 1. cohesion between particles; 2. internal friction between fluid and sediment; 3. turbulence; and 4. inertial impact between particles. The effects of turbulence from non-Newtonian behavior is lumped in the 3rd and 4th terms of the O'Brien et al., 1993 quadratic model combining both turbulent and dispersive forces, which are of key importance in the study. These terms account of the turbulent behavior within the non-Newtonian closure approach. The quadratic model decomposes the stress-strain relationships into the above five components, such that the shear stress is:

$$\tau_{MD} = \tau_{yield} + \tau_{viscous} + \tau_{turbulent} + \tau_{dispersive} + \tau_{Coulomb} \quad \text{(Eq. 3.9.)}$$

where

τ_{MD} = mud-and-debris shear stress (Pa)

τ_{yield} = yield stress (Pa)

$\tau_{viscous}$ = viscous shear stress (Pa)

$\tau_{dispersive}$ = dispersive shear stress (Pa)

$\tau_{turbulent}$ = turbulent shear stress (Pa)

$\tau_{Coulomb}$ = Coulomb shear stress (Pa)

Numerically, these terms are additive, and as concentration increases and as the sediment component coarsens, the library adds terms. This section steps through the cumulative components of each model and is summarized in Figure **6**.

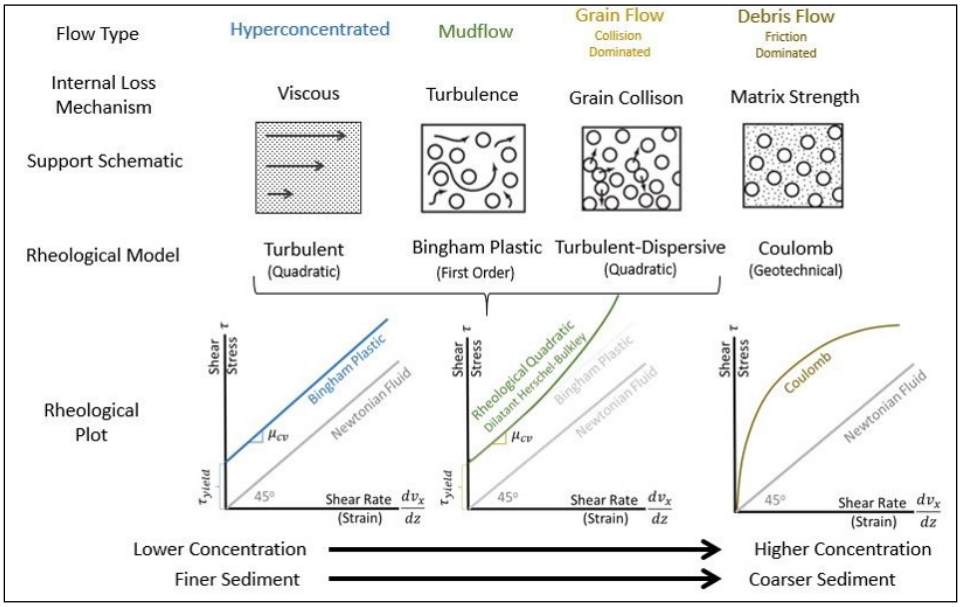

Figure 6. Classification, processes, conceptual model, and rheological model of the four non-Newtonian flow types in the Debris Library.

Bingham Rheology Model. The Bingham model that the library uses to simulate fine-grain dominated mud flows uses the first two terms, such that

$$\tau_{MD} = \tau_{yield} + \tau_{viscous} \qquad \text{(Eq. 3.10.)}$$

This model has a linear stress-strain relationship, with a non-zero intercept. Therefore, the two terms in the shear relationship, τ_{yield} and $\tau_{viscous}$, represent the intercept and the slope, respectively. Therefore, the first order relationship is

$$\tau_{MD} = \tau_{yield} + \mu_m \left(\frac{dv_x}{dz}\right) \qquad \text{(Eq. 3.11.)}$$

Referring to the Bingham model in Figure 6, the yield stress in the intercept and the sediment laden viscosity (μ_m) is the slope of the stress-strain ($\tau \sim \frac{dv_x}{dz}$) relationship. Julien (2010) expresses

the stress in terms of the 1D average downstream velocity ($\bar{u}$) and the flow depth (h) such that

$$\tau_{MD} = \tau_{yield} + \mu_m \left(\frac{dv_x}{dz}\right) = \tau_{yield} + \mu_m \left(\frac{3\bar{u}}{h}\right) \quad \text{(Eq. 3.12.)}$$

Because the hydraulic model generates $\bar{u}$ and h (the depth-averaged velocity and depth), the library must compute the yield stress and the sediment laden viscosity.

Herschel-Bulkley Model. The Herschel-Bulkley (HB) rheology models modifies the Bingham model for fluids that exhibit a non-linear stress-strain relationship, or shear-thinning, can be expressed as

$$\tau_{HB} = \tau_y + K\dot{\gamma}^n \quad \text{(Eq. 3.13.)}$$

Where,

K = fluid consistency index (Pa s^n)

$\dot{\gamma}$ = strain rate (1/s)

n = flow behavior index (-)

Turbulent Quadratic Model Mudflows (non-Newtonian flows composed of dominantly clays and fines grain sediments) have the same viscous dissipative forces as hyperconcentrated flows. However, at these higher concentrations and coarser sediment gradations, inter-particle turbulent losses add an additional term to the momentum equation. Therefore, the shear equation includes a turbulent term for mudflows, such that

$$\tau_{MD} = \tau_{yield} + \tau_{viscous} \quad \text{(Eq. 3.14.)}$$

The turbulent shear is a second order (quadratic) term, making the stress-strain relationship non-linear, such that shear stress increases with the square of strain rate. The quadratic turbulent term is also a function of the density of the mixture (ρ_m) (which is concentration dependent) and the Prandtl mixing length (l_m).

$$\tau_{turbulent} = \rho_m l_m^2 \left(\frac{dv_x}{dz}\right)^2 \quad \text{(Eq. 3.15.)}$$

Julien (2010) approximates the strain (dv_x/dz) as $3\bar{u}/h$, where $\bar{u}$ = the average velocity (m/s) and h = is the flow depth (m), making this term

$$\tau_{turbulent} = \rho_m l_m^2 \left(\frac{dv_x}{dz}\right)^2 = \rho_m l_m^2 \left(\frac{3\bar{u}}{h}\right)^2 \quad \text{(Eq. 3.16.)}$$

Combined with the linear Bingham relationship, this makes the shear-stress relationship a second order polynomial with three terms.

$$\tau_{MD} = \tau_{yield} + \tau_{viscous} + \tau_{turbulent} \quad \text{(Eq. 3.17.)}$$

$$\tau_{MD} = \tau_{yield} + \mu_m \left(\frac{dv_x}{dz}\right) + \rho_m l_m^2 \left(\frac{dv_x}{dz}\right)^2 \quad \text{(Eq. 3.18.)}$$

Therefore, the quadratic model requires two new terms: the mixture density and the Prandtl mixing length. The equation for the Prandtl mixing length is defined as

$$l_m = kz \quad \text{(Eq. 3.19.)}$$

Where, k = the von Karmen coefficient ($\cong$ 0.41) and z = the proportional distance from the boundary (bed).

Turbulent-Dispersive Quadratic Model. As concentration increases, the fluid shear stress (which is used in the friction slope of the hydraulic equations and in the mobility function of sediment transport equations) increases because the mixture density increases, and the slurry mixture gets more viscous.

$$\tau_{MD} = \tau_{yield} + \tau_{viscous} + \tau_{turbulent} + \tau_{dispersive} \quad \text{(Eq. 3.20.)}$$

However, Bagnold (1956) recognized that the diffusive forces in the mixture also change as concentration and grain size increases. As such, the non-Newtonian library computes a dispersive shear stress term of the form (reference unless from Bagnold, 1956).

$$\tau_{dispersive} = 0.01\rho_s \left(\left(\frac{0.615}{C_v} \right)^{1/3} - 1 \right)^{-2} d_s^2 \left(\frac{3\bar{u}}{h} \right)^2 \qquad \text{(Eq. 3.21.)}$$

Where, C_v is the volumentric concentration, and d_s is the representative grain size of the support matrix. The terminology associated with geophysical flows can be confusing with multi-axis gradients complicating this taxonomy. Non-Newtonian fluid behaviour depends on both the sediment concentration and gradation of the solid phase, so the taxonomy usually develops along two axes (that can be, but are not necessarily, correlated). Most classifications (Coussot and Meunier, 1996; Philips and Davis, 1991) categorise these flows based on some relationship between the total solid fraction and the percentage of fine grain solids (i.e., silt and clay or <63 microns). Philips and Davis (1991) quantified this multi-axis organization with the ternary taxonomy provided in Figure 7, modified from Gibson et al. (2020). Because these flows behave differently based on the relative solid and fine content, different rheological and geotechnical models are appropriate to estimate the internal shear (and momentum loss) for different flows.

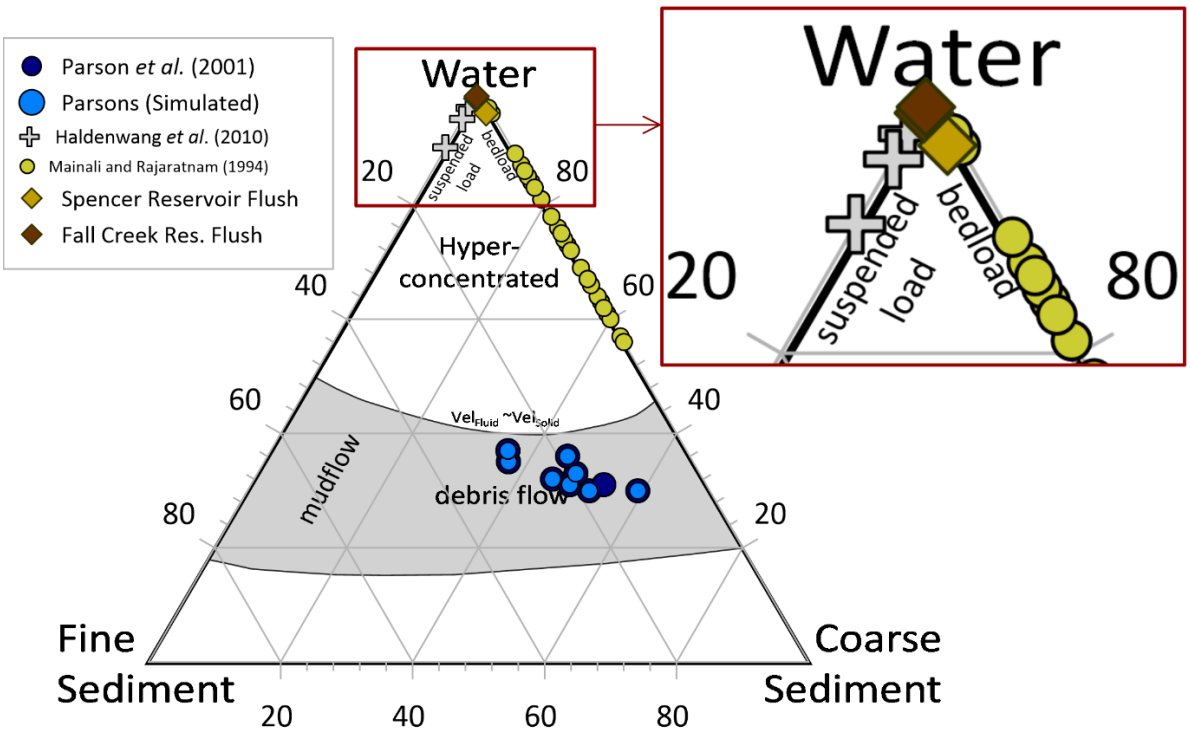

Figure 7. Philips and Davis (1991) ternary classification of geophysical flows with the Parson et al (2001) data (as well as other hyper-concentrated experiments and two reservoir flushes for context) modified from Gibson et al. (2020).

3.2.3. Haldenwang (2003) Flume Experiments

Prediction of Newtonian turbulent flow in open channels has been extensively studied, with non-Newtonian turbulent studies limited to mostly pipe flow conditions (e.g., Mooney, 1931; Govier and Aziz, 1972; Wilson and Thomas, 1985 and 2006). Unlike pipe flow, few attempts have been made to investigate and predict non-Newtonian turbulence for open channel conditions. Naik (1983) investigated flow behavior of Bingham fluids under turbulent conditions, extrapolating Newtonian turbulent approaches for non-Newtonian conditions. More recently, Haldenwang (2003) conducted flume experiment under non-Newtonian turbulent conditions and developed models derived from pipe flow assumption.

In this work, the research team validated DebrisLib within the USACE hydraulic HEC-RAS and AdH numerical models by comparing computed and measured depth and discharge for a range of

geophysical conditions. A selection of experiments from Haldenwang (2003) used to test the non-Newtonian capabilities in these models are plotted on the Phillips and Davies (1991) ternary taxonomy of geophysical flows Figure 7. Of the laboratory test, Haldenwang (2003) covers the lower range of non-Newtonian concentrations, occupying the physical boundary between Newtonian and Non-Newtonian flows. Haldenwang performed a range of flume experiments for a range of fine grain mixtures using both a 10 m long, 0.3 m wide and a 5 m long, 0.15 m wide flume with slopes from 1 – 5 degrees (Figure 8). The low concentrations (Cv = 5-10%) and wide range of flow conditions (laminar, transitional, and turbulent) make these flume experiments particularly useful to evaluate the non-Newtonian approaches in HEC-RAS and AdH.

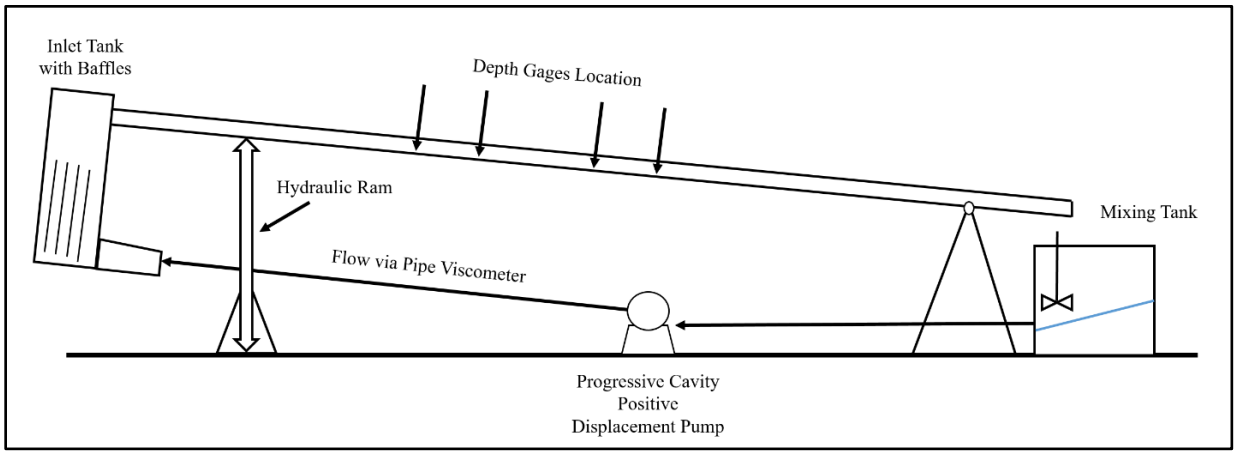

Figure 8. Haldenwang flume configuration.

The flume experiments consisted of measuring discharge with magnetic flow meters and the flow depth with digital depth gauges located at distances of 5 m and 6 m downstream of the inlet. This study simulated conditions in the 10 m long, 0.3 m wide flume for 3°, 4°, and 5° slopes. Table 3 lists the experiment flow and depth conditions for each of the simulated slopes.

Table 3. Experimental Results from Haldenwang (2003) for model calibration. For the 10 percent by volume sediment concentration. Measured at the 6 meter location.

5° Slope Calibration Parameters		**3° Slope Calibration Parameters**	
Discharge (L/s)	Depth (m)	Discharge (L/s)	Depth (m)
20.219	0.0668	20.445	0.1029
18.006	0.0622	18.16	0.0983
16.155	0.0586	16.496	0.0948
14.329	0.0529	14.332	0.0919
12.269	0.051	12.079	0.0892
9.423	0.0471	10.57	0.0862
7.28	0.0414	8.493	0.0867
5.391	0.0394	6.454	0.0836
4.046	0.038	4.202	0.0782
2.945	0.0366	3.418	0.0745
2.25	0.0352	3.286	0.0738
1.487	0.0342	2.293	0.0692
0.913	0.034	1.085	0.0618
0.673	0.0331	0.935	0.0637
0.309	0.0312	0.618	0.0603

The approaches presented in Haldenwang (2003) are useful when determining under what conditions non-Newtonian flows become transitional and then turbulent. Haldenwang (2003) presents approaches for determining the non-Newtonian flow state thresholds based on a modified Reynolds Number derived from pipe theory. For example, turbulent conditions thresholds are defined below for yield plastics (YPP), pseudo plastics (PP), and Bingham plastic (BP) slurries.

$$Re_{(YPP)} = \frac{8\rho_m u^2}{\tau_y + K\left(\frac{2u}{R_h}\right)^n} \qquad \text{(Eq. 3.22.)}$$

$$Re_{(PP)} = \frac{8\rho_m u^2}{K\left(\frac{2u}{R_h}\right)^n} \qquad \text{(Eq. 3.23.)}$$

$$Re_{(BP)} = \frac{8\rho_m u^2}{\tau_y + K\left(\frac{2u}{R_h}\right)} \quad \text{(Eq. 3.24.)}$$

3.2.4. Numerical Modeling Framework

HEC-RAS includes the non-Newtonian algorithms in both the one-dimensional (1D), finite-difference (FD) and the two-dimensional (2D), finite-volume (FV) models. The 1D-FD model requires wet nodes and is not as stable as the FV solution. Therefore, 1D-FD can only simulate a steady-state solution and is not as stable as the 2D-FV solution. As such, only 2D-FV simulations were considered here. The 2D-FV simulation used 3,996 asymmetrical cells aligned with flume flow. RASMapper (the GIS component to the HEC-RAS interface) was used to convert the 1D model cross section into a two-dimensional terrain. Cells were 3 cm long and 1.183 cm wide. This cell width was selected to fit 12 equal-width cells symmetrically across the flume.

The models were initialized with the smallest selectable time step (0.1 s), but HEC-RAS adapted the time step to keep the Courant condition less than 1. This condition reduced time steps to 0.002 or 0.003s (depending on the flow velocity). All simulations used a Manning's roughness coefficient of 0.16, selected before the study based on the sand flume lining and was not calibrated. Traditionally, the 2D model also used mixing and turbulence approaches to compute momentum transfer between cells. The study team estimated the manning n value before simulation, used standard, clear-water mixing parameters, and did not calibrate these parameters. These parameters included a longitudinal mixing coefficient of 0.3, a transverse mixing coefficient of 0.1, and a Smagorinski coefficient of 0.05. These simulations used the full shallow-water equations unless otherwise specified. Because most of the default convergence

and computational tolerances are set for prototype, reach-scale analyses, it was necessary to reduce the values for these laboratory scale flume simulations (10-2 m).

The AdH finite-element (FE) numerical modeling suite is a collection of solvers for the following; unsaturated Richard's equations, Reynolds-Averaged Navier Stokes Equations (RANS), full-momentum shallow-water equations (FMSWE), and the DWE. The FMSWE and the DWE can be meshed in space using Cartesian or spherical coordinate systems. AdH uses the FE method with implicit time stepping to solve the equations of motion and conservation of mass. In AdH the shallow-water equations are discretized using the FE method, in which u, v, and h are represented as linear polynomials on each element. It has been demonstrated that AdH is locally conservative on a control volume for each element (Berger and Howington, 2002). The FE scheme is a streamline upwind Petrov-Galerkin (SUPG) scheme similar to that reported in Berger and Stockstill (1995). AdH has been widely discussed in literature with additional information and details on the model from Savant et al. (2019), Savant et al. (2018), Trahan et al. (2018), Savant and McAlpin (2014), Savant and Berger (2012), and Savant et al. (2011). The AdH mesh was developed using the Surface Water Modeling System (SMS) software including 3300 nodes and 5766 elements with node spacing approximately 0.04 m (Figure 9). The flume was simulated with a small time step of 0.005 s without mesh adaption. As with the HEC-RAS simulations, the Manning's roughness values were determined before modeling and were set to 0.016.

3.2.5. Calculating Results

Haldenwang (2003) reported two observed results: flow depth and discharge. It is vital to compare those observations to the correct simulated results. Since this effort required several simulations and analyzed non-typical results for each, the research team developed MATLAB

scripts to evaluate the models output from all the HEC-RAS and AdH simulations to develop the equivalent computed depths and discharge.

3.3. RESULTS

The research and development team validated Debris Lib within 2D HEC-RAS and AdH by comparing measured discharge and depth to simulated results. Haldenwang (2003) performed numerous experiments with five different slopes, two different widths, two sediment mixtures, and various lower (< 10%) suspended sediment concentrations. This study simulated a selection of those conditions for the large 10-m-long, 0.3-m-wide flume under various slopes. The flume experiments conditions were modeled using three different rheology closures; Bingham, Herschel-Buckley, and Quadratic Model (O'Brien et al., 1993). The 10% Kaolin suspensions had a mixture mass density of 1165 kg/m^3 assuming a grain size of clay approximately 4.0x10^{-5} m. The effort incorporated physical and rheology laboratory measured inputs provided by Haldenwang (2003) and Haldenwang et al. (2010), like yield strength and dynamic viscosity.

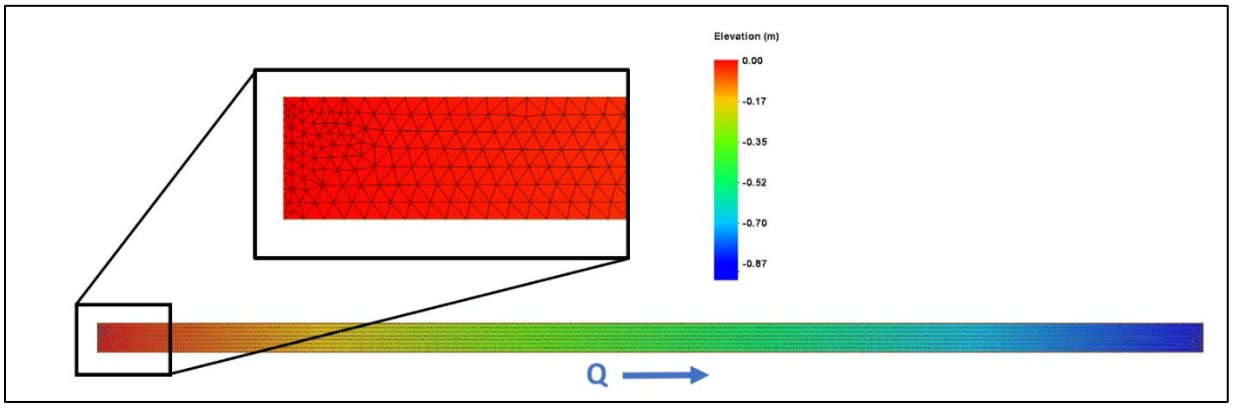

Figure 9. AdH numerical model mesh and bed elevation of Haldenwang (2003) 5 degree 10 m X y m slope flume experiments (from Haldenwang 2003).

In addition, values of yield strength and dynamic viscosity were computed using the empirically derived approach from O'Brien and Julien (1988), O'Brien et al. (1993), and Julien (2010). The physical and rheology properties used in the HEC-RAS and AdH simulations can be found in

Table 4. The 5 degree slope modeled results are provided in Figure 10 and Figure 11 for HEC-RAS and AdH, respectively.

Table 4. Physical and rheology properties used in numerical simulations of Haldenwang (2003) flume experiments. All parameters are laboratory derived.

	Properties				
Rheology Closure	Yield Strength (Pa)	Dynamic Viscosity (Pa s)	Fluid Consistency Index (Pa s^n)	Flow Behavior Exponent (-)	Grain Size (m)
Bingham Model	21.3	0.00316	-	-	-
Herschel-Buckley (H-B)	21.3	-	0.00275 (n=1) 0.524 (n< >1)	0.468	-
Turbulent Quadratic Model (TQM)	21.3	0.00275	-	-	$4.0x10^{-5}$

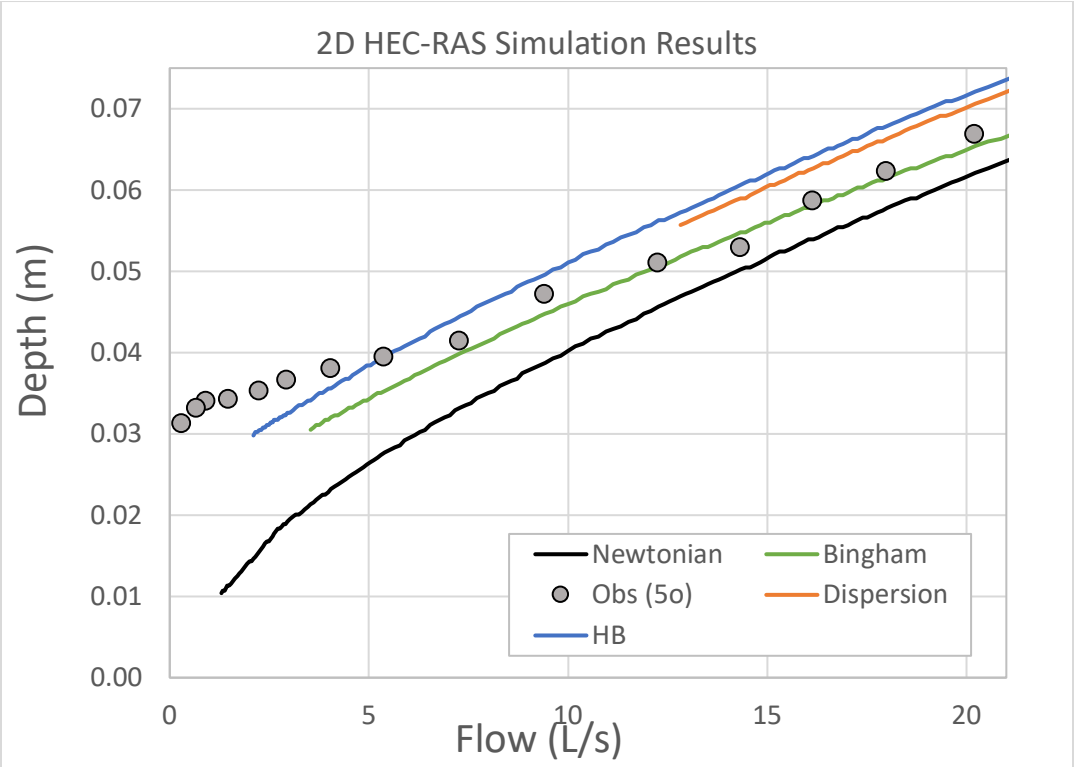

Figure 10. Simulation of Haldenwang (2003) 5 degree slope flume using 2D HEC-RAS with one Newtonian viscosity condition and three non-Newtonian rheology closures.

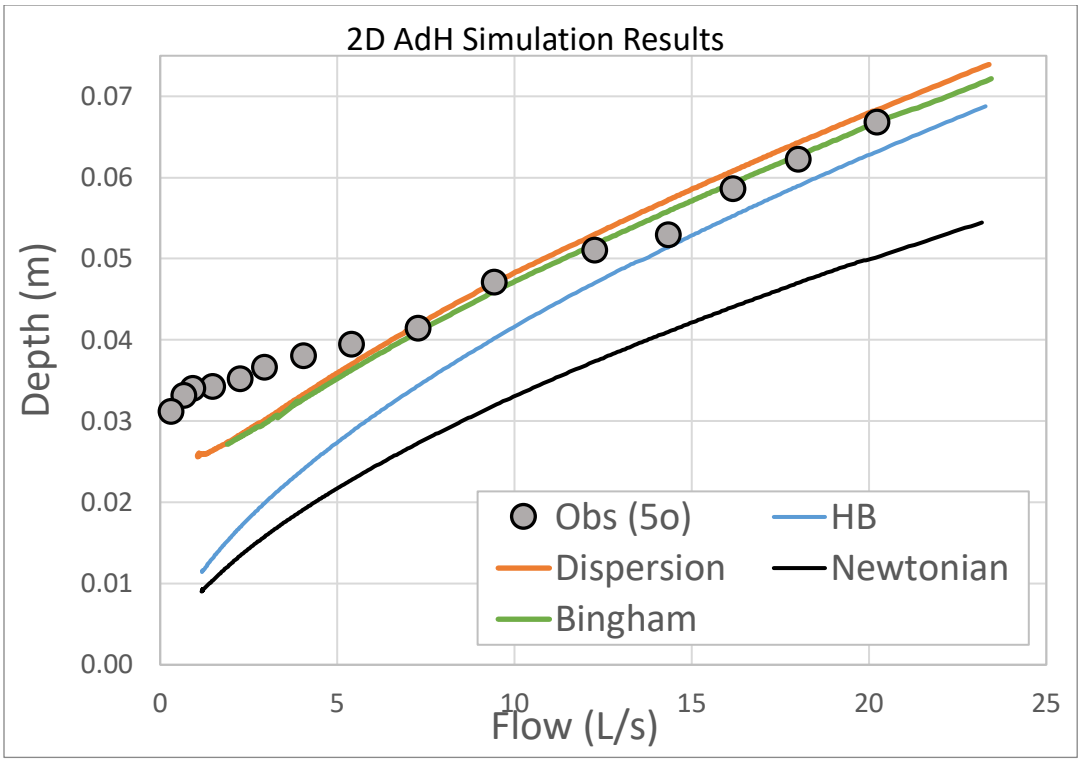

Figure 11. Simulation of Haldenwang (2003) 5 degree slope flume using 2D AdH with one Newtonian viscosity condition and three non-Newtonian rheology closure.

3.4. DISCUSSION

All of the non-Newtonian simulations in Figure 10 and Figure 11 out-performed the Newtonian simulations, indicating that even at 10% sediment concentration by volume Newtonian physics are inadequate at predicting both flow and depth. The Newtonian results under predict both flow and depth for the entire flume experiment conditions. However, the results still deviated from observed discharge and depth in a few cases. The non-Newtonian model simulations tended to under-predict the lower discharges and more adequately predict the higher discharges. The simulated discharge and depth residuals are larger likely for low flow rates due to the strain rate definition in the non-Newtonian closure library. HEC-RAS, AdH, and DebrisLib incorporate a strain rate approximation, derived assuming a parabolic velocity profile that likely deviates from the physical conditions Haldenwang (2003) measured during the flume experimental conditions. The approach presented here computes strain rate from the ratio of the velocity and depth in each

computation cell or element, defined as $3u/h$, based on O'Brien et al., 1993 assumption. This difference in strain rate approximation explains most of the computation residuals, despite incorporating laboratory measured physical and rheology parameters (e.g., Haldenwang, 2003). The Haldenwang (2003) experiments provide an ideal dataset to evaluate the lower sediment concentration limits of single-phase shallow-water rheology-based non-Newtonian closure. The range of flow behavior (laminar, transitional, and turbulent) from these experiments generate conditions which can complicate numerical modeling of multi-phase non-Newtonian flows with a single-phase rheological modeling approach.

It's critical to understand the differences between laminar and turbulent flow and how they are represented within the numerical models HEC-RAS and AdH. Ideally, this partition between flow conditions could be computed as a function of a non-Newtonian based Reynolds Number as identified by Haldenwang (2003). The variability seen between the model results and the flume experiments indicate the models adequately represent both flow and depth for most flow conditions. Interestingly, all the rheology closures within the numerical models were able to predict the turbulent and transitional flow conditions better than the lower energy laminar flow. We also hypothesize that the differences might also be the result of the development of a 'partition' or lutocline within the flow column, potentially resulting in development of non-Newtonian bedload and suspended load processes (Takahashi et al., 1992). This could not be confirmed due to the lack of vertical velocity profile information, but this hypothesis will be tested in future research. We propose that in transitional and turbulent conditions, the flow fully entrains the fine sediment resulting in a single phase flow type velocity and concentration profile (likely parabolic in shape) with no physical discernable variation in concentration with depth, similar to the non-Newtonian numerical model assumptions presented here. Conversely, during

laminar flow conditions these concentration 'layers' may exhibit different resistance properties as described by Takahashi (2001). This verifies the importance in distinguishing when single-phase model assumptions are invalid and highlights the need for continued model validation and parameterization to develop efficient, yet adequate approaches to account for the variability shown at the lower flow conditions.

3.5. CONCLUSION

This research is focused on improving representation of potential post-wildfire flood conditions, at the lower bound of non-Newtonian hyperconcentrated flows. All simulations using non-Newtonian rheology closures in DebrisLib had considerably better results, compared to the flume experimental data, than the Newtonian equations. This research provides a foundation to develop a better understanding of non-Newtonian turbulence in the role of rheology based models to predict a range of flow conditions commonly seen in post-fire flooding. In addition, this work will facilitate development of a formal approach for determining what type of non-Newtonian model closure is appropriate for predicting laminar, transitional, and turbulent conditions. Furthermore, this confirms the importance of considering non-Newtonian flow physics, even at lower non-Newtonian sediment concentrations. Post-wildfire flooding and other geophysical flows are becoming more common and pose a unique challenge for the flood risk management community. A validated, broadly applied model with non-Newtonian mud and debris flow capabilities will aid the flood risk and emergency management communities to better manage these risks. These non-Newtonian approaches are currently available in HEC-RAS and AdH, with DebrisLib capable of connecting to other research and operational-level software platforms. However, broader application of these algorithms requires evaluation of the assumptions of each approach, and testing of the parameters for each situation.

CHAPTER 4. EVALUATION OF POST-WILDFIRE HYDROLOGIC AND HYDRAULIC MODELING APPROACH FOR FLOOD RISK MANAGEMENT

4.1. INTRODUCTION

Following the 2017 Thomas Fire early on 09 January 2018 an intense precipitation event above Montecito, CA produced debris flows from the steep watersheds in the Santa Ynez Mountains. After exiting the mountain front the debris flows traveled approximately 3 km downstream across a series of alluvial fans killing 23 people and significant destruction of residential structures and infrastructure. The occurrence and intensity of wildfires in the arid and semi-arid western U.S. has become a major concern over the past decade. These intense and large wildfires, specifically in fragile ecosystems, can represent a significant shock (or change) to the natural system and significantly modify the hydrology, ecology, and geomorphology for several years following the fire. The results of wildfires produce varying spatial effects across the effected watershed and alter hydrology through the removal of vegetation and ground cover, production of ash layers, reduction of organic material in soils, alteration of soil structure, disaggregation of soils, and development of hydrophobic soils. Wildfires change the infiltration properties of soils and reduce the amount of interception material such as canopy, litter, duff, and organic material which protect soil from raindrop impact and slow runoff (Moody & Martin, 2001). Infiltration commonly decreases due to changes in the chemical (Debano & Dunn, 1969) and physical (Wells, 1981) properties of the soil, making the soil hydrophobic (water-repellent). Unit-area peak discharges measured following a wildfire have been shown to increase 1.5 to 870 fold over pre-fire peak discharges (Moody & Martin, 2001).

As a result, these effected environments can experience a wide range of hydrologic and hydraulic responses from no response, to increased runoff, and development of destructive non-Newtonian

debris flows and floods. In mountainous arid and semi-arid regions non-Newtonian flows can be the typical response following large intense wildfires (Burns and Gabet, 2015). The mechanisms for the generation of runoff driven non-Newtonian flows are not fully understood quantitatively, but two factors appear necessary for generation of post-wildfire debris flows: sufficient runoff and mobile soils, sediments, and woody debris (Cannon, 2001; Cannon et al., 2001b; Burn and Gabet, 2015). These non-Newtonian mudflows, debris flows, and 'ash' flows are unsteady gravity-driven events that involve complex mixtures of sediment, water, and entrained material (i.e., organics, woody debris, unconsolidated substrate). These non-Newtonian flows have high sediment concentrations (5% - 83% volumetric concentration) and can carry large boulders, trees, and uprooted infrastructure (e.g., upstream structures or bridge debris). These conditions violate the assumption of Newtonian hydraulic shallow-water models requiring models derived from non-Newtonian physics.

Post-wildfire hydrographs are challenging to predict because of limited quantitative understanding of physical processes mechanics and limited availability of dynamic datasets (e.g., flow, depth, and velocity) (Moody et al., 2008a). These flood events are notoriously challenging to measure as a result of intense erosion and deposition processes, and often damage or destroy gaging equipment and instrumentation (Moody et al., 2013). As a result, Moody et al. (2013) identified from the literature more heuristic, empirically-based approaches, specifically: 1) paleo-flood methods (e.g., Jarrett and England, 2002), 2) curve number approach (e.g., Hawkins and Greenberg, 1990; Foltz et al., 2009), or 3) direct measurements from burned watersheds (Moody and Martin, 2001a; Moody et al., 2008a; Kean et al., 2011; Moody, 2012). Previous approaches predicting post-wildfire flood risk (Burn et al., 2007; Cannon and Gartner, 2005; Cannon et al., 2010; Bernard, 2007; Moody et al., 2013) are limited to mostly empirical regression approaches

to predict debris flow potential and estimate sediment volume for a given watershed or sub-basin outlet for a given range of precipitation events (e.g., Cannon et al., 2010), and do not address dynamic prediction of downstream runout and inundation. These empirical approaches are simple and useful for hazard warning, emergency response, and management but have limitations, and are restricted to use in watersheds with similar physiography, geology, ecological, and climate conditions.

Unfortunately, few researchers have focused on predicting post-wildfire flood velocity, depth, and downstream inundation (Elliot et al., 2010; Moody et al., 2013). More specifically, no existing operational numerical models are capable of predicting both Newtonian and non-Newtonian physics within a single model. Existing non-Newtonian models vary widely (e.g. Jin and Freed, 1999; O'Brien et al., 1993; Iverson, 1997; Naef et al., 2006) with varying model assumptions, solution procedure, and complexity. The primary purpose of this research was to simulate the 09 January 18 debris flow events documented in Kean et al., 2019 to evaluate the effectiveness of the non-Newtonian DebrisLib with the two-dimensional HEC-RAS models at predicting post-wildfire non-Newtonian (e.g., debris flow, mudflows, hyperconcentrated flows) flow conditions.

4.2. SITE AND EVENT CHARACTERISTICS

The County of Santa Barbara is located in southern California part of the California Central Coast. The impacted watersheds analyzed as part of this study are Montecito Creek and San Ysidro Creek, as well as the associated tributaries. The watershed span the peaks of California's Transverse Ranges that exceed 1,100 m in elevation and drain into the Pacific Ocean a few kilometers downstream. The steep gradients from the ocean also leads to strong orographic effects resulting in intense rainfall events. The vegetation is predominately chaparral and tends to

burn in volatile wildfires resulting in highly disaggregated, erodible, and hydrophobic soils. The combination of steep gradients, intense precipitation, and susceptibility for wildfires make the Transverse Ranges particularly vulnerable to destructive non-Newtonian flood events.

On 4 December 2017 the Thomas Fire began on the southern slopes along State Route 150 above Santa Paula, California. The fire then burned west and north through eastern Ventura County and southwestern portions of Santa Barbara County (Figure 12). The fire burned approximately 282,000 acres, with full containment not declared until 12 January 2018. Subsequently, on 9 January 2018, a winter storm produced an estimated 0.5 inches of precipitation falling within a five-minute period (as recorded by the Montecito Creek rain gauge) at approximately 0330 PST, representing a rainfall intensity with a 0.2% to 0.5% annual percent chance exceedance. This intense precipitation event on the recently burned mountainous terrain caused a series of debris flows to surge downstream from the Santa Ynez Mountains into the communities of Montecito, Summerland, and Carpinteria, resulting in significant damage to life and infrastructure. This research presents the results from hydrologic modeling, hydraulic modeling, sediment yield, and sedimentation analysis for Montecito Creek and San Ysidro Creek (Figure 13).

Figure 12. Location map of the 2017 Thomas Fire burn extent effecting portions of Santa Barbara and Ventura Counties, CA (red line indicates burn extent).

Figure 13. Site location of post-wildfire impacted watersheds near Santa Barbara (Montecito and San Ysidro Creeks indicated in red).

4.3. POST-WILDFIRE HYDROLOGY AND HYDRAULIC CONCEPTUAL MODEL

Immediately following a wildfire, vegetation is removed, organic soil horizons are reduced to ash, and soils may turn hydrophobic, which combined result in increased hillslope surface runoff and development of debris flows and similar analogous non-Newtonian flows (Cannon et al., 2001; Moody et al., 2013; Kean et al., 2019). With Figure 14 providing additional post-wildfire effects on hydrology and hillslope processes.

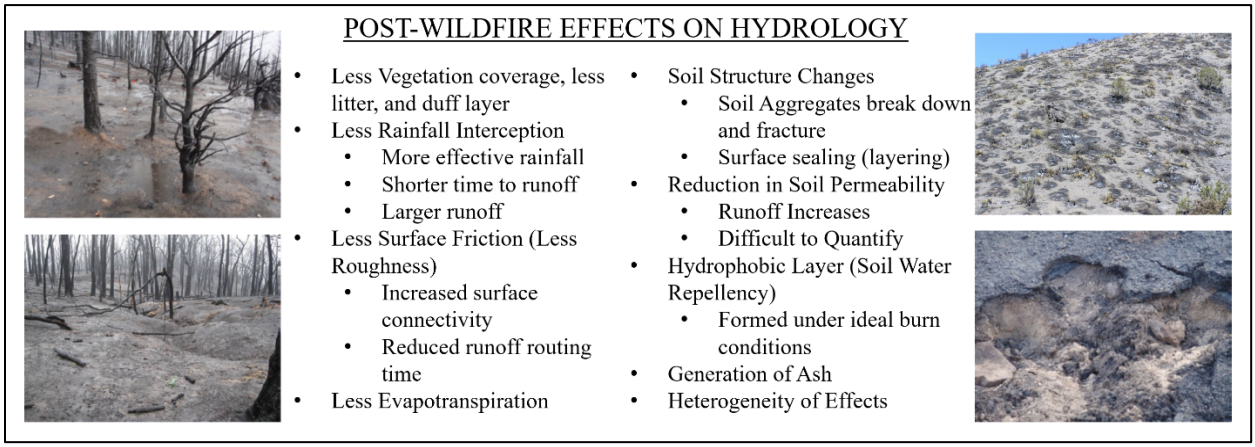

Figure 14. Post-wildfire effects on soils and vegetation altering hydrology processes.

Post-wildfire flood events can also exhibit both Newtonian and non-Newtonian behavior requiring operational (or engineering) decision making tools and models to account for both types of flood behavior. Most existing hydrology rainfall-runoff models commonly use: 1) empirical-based regression equations or 2) curve number methods (Moody et al., 2013; Foltz et al., 2009). Both rainfall-runoff approaches have issues for accounting for wildfire effects identified in Figure 14. Application of the curve number method for post-wildfire watersheds has produced inconsistent result with additional research needed (Springer and Hawkins, 2005; Moody et al., 2013). These approaches require a channel routing hydrodynamic model that can account for both Newtonian and Non-Newtonian flow runout dynamics and downstream inundation (e.g., Pradhan et al., 2019). A diagram of the hydrology and hydraulic conceptual model is provided in (Figure 15). The conceptual model integrates engineering-based hydraulic

numerical models to account for downstream runout and floodplain inundation using input post-wildfire hydrology sediment runoff yields. In Figure 15 below the map view diagram (on left), the grey area represents the hydrology and hillslope model domain with the green area indicating the downstream hydraulic model area. Output boundary conditions from the parent hydrology model provides the input boundary conditions to predict the downstream runout and inundation using either classic Newtonian physics or non-Newtonian closure. The boundary between the hydrology and hydraulic models can be defined based on location of human made infrastructure and natural features, to include: geomorphology/geology features, changes in slope (typically dependent on the hydraulic model slope limitations), and infrastructure (e.g., debris basin outflow, reservoirs, flood control structures, etc.).

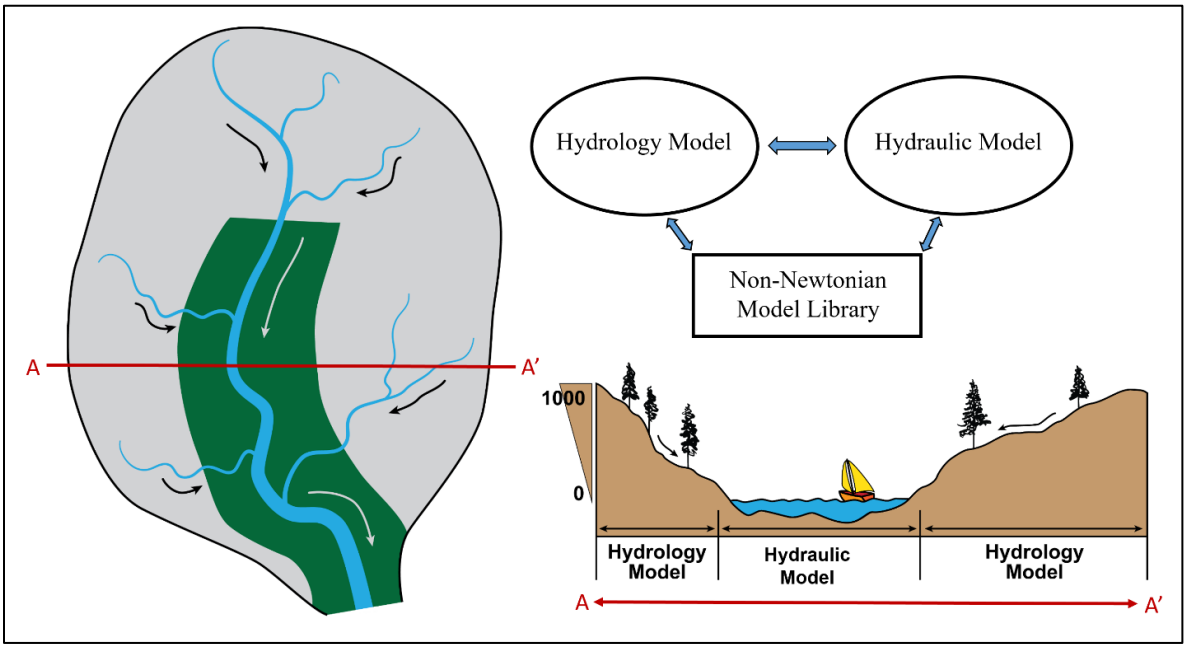

Figure 15. Conceptual hydraulics and hydrology post-wildfire conceptual model.

Currently, few hydrology or hydraulics software packages have the capability to simulate both processes, and those that do are typically research-focused codes and not used in standard practice. This modeling can be achieved through the use of the non-Newtonian modular library

'DebrisLib' linked with a given parent hydrology or hydraulic software to account for both Newtonian to non-Newtonian flow using non-dimensional thresholds from Lan and Julien (1991), Iverson and Denlinger (2001), and Julien (2010). As part of the post-wildfire fire conceptual model, the hydrology and hydraulic parent codes are linked with the non-Newtonian modular library 'DebrisLib' to account for both hydrodynamic non-Newtonian processes.

The non-Newtonian model library DebrisLib allows the user and/or parent program to select a specific non-Newtonian model (e.g. Bingham; O'Brien et al., 1993; Hershel Bulkley). The library can also select the appropriate closure model, based on the physical conditions, which is particularly useful if the flow type changes over time or space, making a single model inappropriate. Additional details on the non-Newtonian library, DebrisLib, can be found in Floyd et al. (2019), Pradhan et al. (2019), and Gibson et al. (2020). Pradhan et al. (2019) presents a generic flow diagram describing the linkage-architecture of DebrisLib and a hydrologic or hydraulic parent code. The approaches presented here are only conceptual in nature and will require additional research and development to evaluate and demonstrate the approach validity and range of application. As shown in Figure 16 first the flow is classified as Newtonian or non-Newtonian. If the flow is Newtonian then standard parent code approach is used. If the flow is determined to be non-Newtonian then additional dimensionless parameters are used to determine the type of non-Newtonian flow and then apply the most appropriate closure.

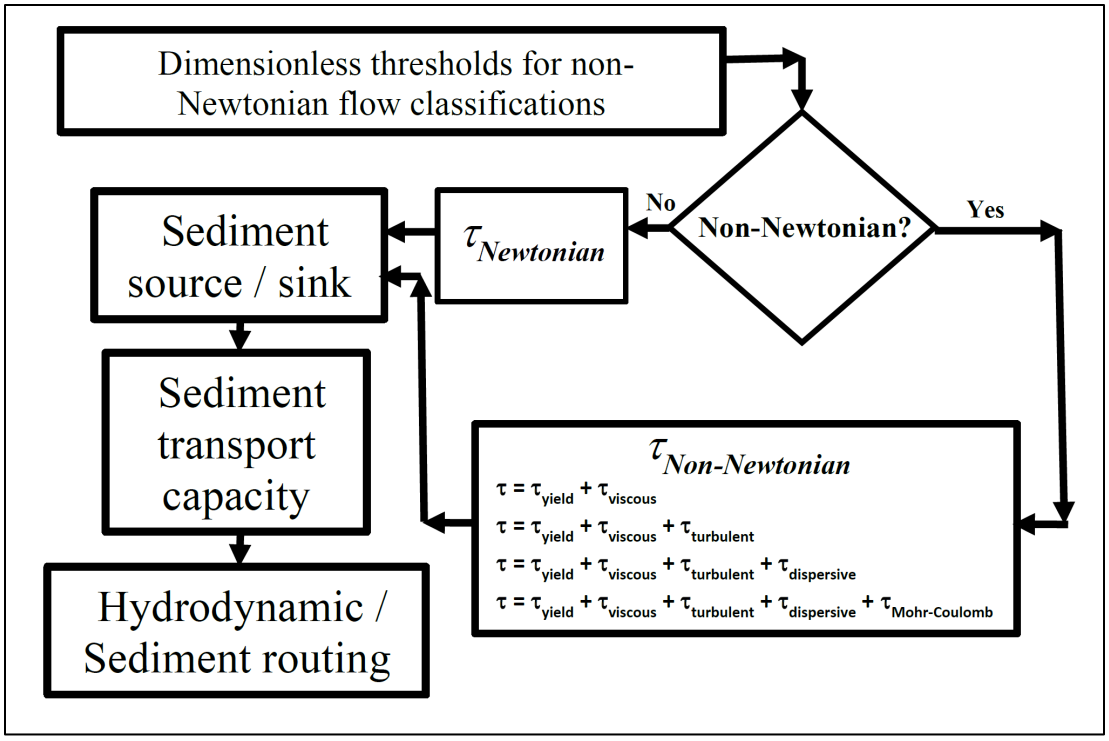

Figure 16. Non-Newtonian modelling flow diagram (modified from Pradhan et al., 2019).

Physically representing the flow classification involves additional variables, to include concentration, grain size, and flow depth and velocity, dynamic viscosity, and particle density using non-dimensional parameters. The library computes five dimensionless terms to determine the non-Newtonian flow type:

1. The Viscous Parameter (Julien, 2010)

$$N_{Viscous} = \frac{\tau - \tau_{yield}}{\mu_m \left(\frac{3\bar{u}}{h}\right)} \qquad \text{(Eq. 4.1.)}$$

2. The Turbulent Parameter (Julien, 2010)

$$N_{Turbulent} = \frac{l_m^2 \rho_m}{0.01 d_s^2 \rho_s} \left(\left(\frac{C_{max}}{C_v}\right)^{\frac{1}{3}} - 1 \right)^2 \qquad \text{(Eq. 4.2.)}$$

3. The Dispersive Parameter (Julien, 2010) is very similar to the dispersion shear, except that the sediment laden viscosity is included in the denominator and the strain is not squared, to make the parameter dimensionless.

$$N_{Dispersive} = \frac{0.01\rho_s d_s^2}{\mu_m}\left(\left(\frac{C_{max}}{C_v}\right)^{\frac{1}{3}} - 1\right)^{-2}\left(\left(\frac{3\bar{u}}{h}\right)\right) \quad \text{(Eq. 4.3.)}$$

4. The Savage Number (Iverson and Denlinger, 2001) is the ratio between inertial shear stress from grain collisions and grain friction (Coulomb) and determines the difference between collision dominated and friction dominated flows in coarse material.

$$N_{Savage} = \frac{\rho_s\left(\frac{3\bar{u}}{h}\right)^2 d_s}{(\rho_s - \rho)gh\tan\phi} \quad \text{(Eq. 4.4.)}$$

5. An additional useful non-dimensional parameter from Iverson (1997) is the friction number defined as the ratio of frictional to viscous forces. The friction number can be approximated by

$$N_{friction} = \frac{C_v(\rho_s - \rho)gh\tan\phi}{(1 - C_v)\left(\frac{3\bar{u}}{h}\right)\mu_m} \quad \text{(Eq. 4.5.)}$$

where, ϕ = internal friction angle (°). The library uses these numbers to classify the flow conditions for each cross-section or node and determines which equation or combination of equations are the most appropriate. The hypothesized flow condition and associated non-dimensional thresholds are summarized in Table 5 and Figure 17. These threshold ranges were compiled from published research by Julien and Lan (1991), Iverson (1997), and Julien (2010).

Ongoing research is focused on validating these parameter threshold validity but is challenging requiring gage data collected from across effected watershed.

Table 5. Non-Dimensional thresholds for flow conditions.

Flow Conditions	**Thresholds**
Newtonian Flow	$N_{viscous} < 1$
Hyperconcentrated Flow	$1 < N_{viscous} < 5$
Mudflow	$N_{viscous} > 5; N_{turbulent} > 1$
Hyperconcentrated Grain Flow	$N_{viscous} > 5; N_{dispersive} > 4$
Debris Flow	$N_{Savage} < 0.1; N_{friction} > 100$

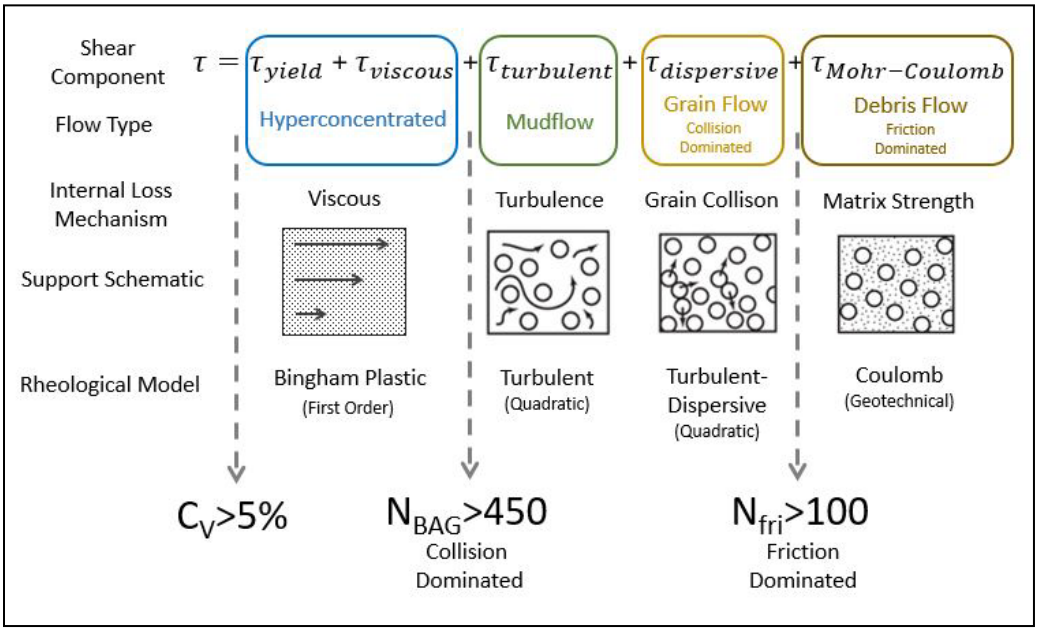

Figure 17. Non-Newtonian flow classification, process, and conceptual model with non-dimensional thresholds.

4.4. METHODOLOGY

4.4.1. Hydrology Modeling Approach

The watersheds were delineated based on the location of stream gauges, major confluences, basins damaged by the Thomas Fire, and locations that coincided with areas of transition

between hydrology and hydraulic models. Existing HEC-HMS hydrology models were modified to represent the 2017 Thomas Fire conditions based on the Burned Area Emergency Response (BAER) assessment. Runoff and erosion from the watersheds were predicted using the Modified Universal Soil Loss Equation (MUSLE) (Williams, 1975). Hydrology in channel sediment routing was not considered, as all in channel modeling was conducted with two-dimensional HEC-RAS. Post-wildfire event-based sediment data and yields from Kean et al., 2019 were, for calibration, available as estimated by volume of excavated material from select debris basins and downstream floodplain reaches in the affected areas. The rainfall runoff and sediment yield model results were calibrated against estimates of material excavated from recent flood events.

Additional sediment yield was available from USGS surveys, as detailed in Kean *et al. (*2019). The volume of deposited material within the floodplain was used to calibrate the watershed hydrology and sediment yield models. The Kean et al. (2019) data provided flow surface elevations measured from the flood event mudlines on trees and infrastructure across the inundation areas from the 2018 debris flow event. These datasets provide the foundation for model validation. Sediment grain size distributions curves were developed from field samples and data collected across the model domain. Only the Montecito watershed had gage data available so the initial HEC-HMS model conditions were first calibrated for Montecito and extrapolated to the adjacent San Ysidro watershed model. Additional details on the HEC-HMS model calibration can be found in USACE (2020).

Within HEC-HMS, the vegetation cover factor was adjusted to calibrate runoff curve number estimation, until the sediment yields matched estimates from Kean et al. (2019) and estimates of material removed from filled debris basins. The vegetation cover factor was one of the most uncertain variables in the curve number approach with increased runoff due to wildfire effects on

vegetation and ground cover. This variable was adjusted to more adequately represent the loss of vegetation following a wildfire. To apply this approach to the other watersheds, hydrologic parameters had to be developed for the ungauged watersheds. Once the hydrologic parameters were determined, the sediment yield calibration was repeated, as described in USACE (2020). The HEC-HMS Newtonian discharge output was then bulked using a simple analytical approach to account for the increased sediment load. Richardson (2001) defines bulking as increasing the water discharge to account for the increased concentrations within the flow, in part due to increase erosion potential and effects of hindered settling on deposition. The bulked flow was computed as a function of concentration and applied to the hydrograph to estimate the total water-sediment discharge (WEST, 2011; Floyd et al., 2019). The bulked flow is defined as water discharge divided by one minus volumetric concentration. Initial conditions for the HEC-RAS models were bulked using a range of sediment concentration from 40% to 70% by volume.

4.4.2. Hydraulic Modeling Approach

Typically hydrodynamic and sediment models predict flow with the shallow-water depth-averaged equations, which combine the conservation of mass and momentum equations and assume Newtonian conditions to solve for velocity and depth. Recently, HEC-RAS software has been linked with the non-Newtonian 'DebrisLib' model library (Floyd et al., 2019; Gibson et al., 2020) for both 1D and 2D solvers, with this paper only focusing on the 2D results. The approach can solve either the depth-averaged shallow-water equations (SWE) or the diffusion wave equation (DWE). The SWE version solves both volume and momentum conservation equations including both spatial and temporal accelerations and horizontal mixing. The DWE approach ignores XX and YY and while simpler and more computationally efficient, is limited in ZZ. The conservation of mass equation is given by

$$\frac{\partial \eta}{\partial t} + \nabla \cdot (hu) = q \qquad \text{(Eq. 4.6.)}$$

where,

η = the flow water surface elevation (m)

t = time

h = flow depth (m)

u = velocity vector

q = source/sink term

The depth averaged conservation of momentum equations are defined as

$$\frac{\partial u}{\partial t} + (u \cdot \nabla)V = -g\nabla\eta + \frac{1}{h}\nabla \cdot (v_t h \nabla u) - c_f u - \frac{\tau}{\rho_m h}\frac{u}{|u|} \qquad \text{(Eq. 4.7.)}$$

where,

g = the gravitational acceleration,

v_t = turbulent eddy viscosity,

c_f = bottom friction coefficient,

τ = the non-Newtonian internal stress,

ρ_m = the density of the water-solid mixture, and

$|V|$ = the magnitude of the velocity vector.

The second term on the right-hand side of the conservation of momentum equation characterises horizontal mixing due to turbulence and in the case of non-Newtonian flow horizontal mixing due to particle collisions. DebrisLib modifies key variables within Equation 4.7 using approaches to estimate non-Newtonian internal stress, mixture mass density, dynamic viscosity, and eddy viscosity. The implicit solution procedure of HEC-RAS then determines the non-Newtonian

depth and velocity during the subsequent time step. Using the conservative form of the mixing equations is critical for accurate prediction of conservation of momentum. The boundary friction coefficient is computed based on the Manning's roughness coefficient, define as

$$c_f = \frac{gn^2}{R^{\frac{4}{3}}}|u| \qquad \text{(Eq. 4.8.)}$$

where, R is the hydraulic radius and n is the Manning's roughness coefficient. HEC-RAS also solves a simplified, unsteady hydraulic model replacing the conservation of momentum equation with the DWE, define as

$$\frac{\partial \eta}{\partial t} + \nabla \cdot (\beta \nabla \eta) = q \qquad \text{(Eq. 4.9.)}$$

Where, β is a non-linear coefficient which is a function of the bottom friction and non-Newtonian internal stress

$$\beta = \frac{K}{A}\frac{R}{|\nabla \eta|^{\frac{1}{2}}} \qquad \text{(Eq. 4.10.)}$$

where,

$$\frac{K}{A} = \left(\frac{n^2}{R^{\frac{4}{3}}} + \frac{\tau}{\gamma_m R|u|^2}\right)^{-\frac{1}{2}} \qquad \text{(Eq. 4.11.)}$$

where,

K = the conveyance,

A = the vertical area, and

γ_m = the unit weight of the water-solid mixture.

The two-dimensional HEC-RAS hydraulic models were developed for the Montecito and San Ysidro creeks. The HEC-RAS computational mesh was developed based on the floodplains boundaries for each watershed determined using USGS data collection following the 09 January 2018 flood event (Kean et al., 2019) and publically available GIS data. The HEC-HMS results provide the upstream hydrodynamic boundary condition for the two-dimensional HEC-RAS non-Newtonian simulation. The mesh resolution was 15 m by 15 m and extended from the upper watershed to the Pacific Ocean. The effects of blocking of infrastructure (e.g. bridges and culverts) and avulsions were considered in model development. These structures were documented across the impacted watersheds (Kean et al., 2019) and were addressed using a serious of 'rules' to estimate blockage then dynamically simulate the avulsion. The non-Newtonian prediction in HEC-RAS requires estimation of several key parameters like volumetric sediment concentration, yield strength, dynamic viscosity, and empirically determined coefficients. Sediment concentration was measured with the other variables approximated using the equations and recommended coefficient from O'Brien et al., 1993. The sediment concentration was estimated by Kean et al., 2019 through post-event data collection and ranged from approximately 30% to 70% by volume. The other variables yield strength and dynamic viscosity were estimated using the empirical approach from O'Brien et al., 1993 with coefficients determined based on data from laboratory and field data (O'Brien et al., 1993; Julien, 2010) based on typical soil ranges. The approach taken here assumes a constant concentration (constant yield strength, viscosity) and fixed bed conditions. While these assumptions introduce issues and limitations for capturing dynamic variables like depth and velocity and the potential for significant sediment erosion and deposition, it allows us to focus solely on understanding how incorporation of non-Newtonian processes impacts the flood

downstream runout and inundation. Future research is needed to extend the range and number of processes included.

4.5. RESULTS

4.5.1. Hydrology Modeling

A discharge-frequency relationship was established for San Ysidro Creek from an existing USGS gauge. Since all the watersheds are adjacent to each other we assume they have similar hydrologic characteristics (meteorological, land-use, terrain, etc.). The discharge-frequency relationship developed for San Ysidro Creek (USGS 11119660) was weighted by the quantity of watershed drainage area to produce the estimates for Montecito and San Ysidro Creeks. The hydrology calibration results for 2019 Montecito Creek flood events are shown in Table **6** with the sediment yield calibration results for the 09 January 2018 events in Montecito and San Ysidro creeks are shown in Figure 18.

Table 6. Montecito Creek Hydrologic Calibration Results.

Flood Events	Nash-Sutcliffe Efficiency	Peak Discharge Modeled (m^3/s)	Volume Modeled (m^3)	Peak Discharge Observed (m^3/s)	Volume Observed (m^3)
2-Feb-19	0.669	46.66	3.586E+05	77.81	2.948E+05
14-Feb-19	0.877	14.12	1.680E+05	14.13	1.526E+05
17-Jan-19	0.674	28.45	3.753E+05	17.10	3.689E+05
6-Jan-19	0.657	2.98	8.166E+04	4.66	5.082E+04
31-Jan-19	0.817	20.22	1.340E+05	25.50	1.332E+05

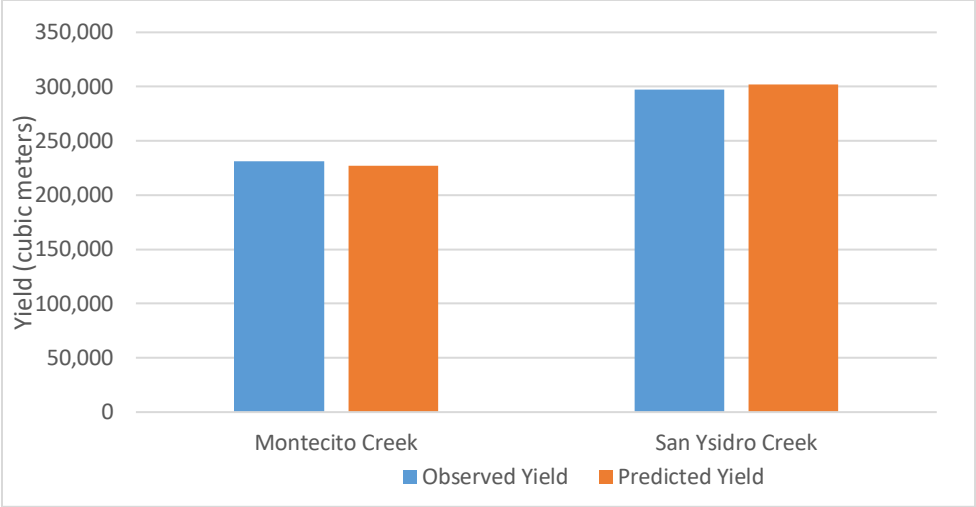

Figure 18. 2018 Post-wildfire Event Sediment Yield Calibration Results (Observed values from Kean et al., 2019 and Debris Basin Excavated Estimated Volumes).

The pre- and post-wildfire HEC-HMS flow results for various AEPs for Montecito and San Ysidro Creeks are shown in Table 7 and Table 8, and were applied as the upstream boundary condition in the Montecito and San Ysidro Creek two-dimensional HEC-RAS hydraulic models. Currently, the HEC-HMS model doesn't account for the effects of high sediment concentration or non-Newtonian behavior during routing. The clear-water discharges simulating the 09 January 2018 events were bulked using peak volumetric concentration to approximate the effects of high sediment concentrations on flow mechanics.

Table 7. Summary of HEC-HMS Flow Results for Montecito Creek watershed based on 09 January 2018 conditions.

Annual Exceedance Probability	HMS Pre-Wildfire Flow (m^3/s)	Post-Wildfire HMS Flow (m^3/s)	Percent Increase
0.2%	243.89	282.83	16.0%
0.5%	182.98	217.79	19.0%
1.0%	139.80	169.31	21.1%
2.0%	103.90	128.08	23.3%
4.0%	72.35	89.93	24.3%
10.0%	37.55	49.61	32.1%
20.0%	18.49	24.64	33.3%
50.0%	4.22	8.41	99.8%

Table 8. Summary of HEC-HMS Flow Results for San Ysidro Creek watershed based on 09 January 2018 conditions.

Annual Exceedance Probability	HMS Pre-Wildfire Flow (m^3/s)	Post-Wildfire HMS Flow (m^3/s)	Percent Increase
0.2%	154.38	181.82	17.8%
0.5%	116.55	143.96	23.5%
1.0%	88.32	109.76	24.3%
2.0%	65.67	83.31	26.8%
4.0%	46.24	59.58	28.8%
10.0%	24.27	32.48	33.9%
20.0%	12.15	16.65	37.0%
50.0%	2.63	4.42	68.8%

4.5.2. Hydraulic Modeling

The hydraulic two-dimensional HEC-RAS models were used to simulate the 09 January 2018 Thomas Fire flood and debris flow events by varying the Manning's Roughness and non-Newtonian rheology parameters until agreement between simulated inundation area and the observed inundation area using the Kean et al. (2019) inundation data. The roughness coefficients were determined from the 2016 National Land Cover Database and building locations and footprints ranging from 0.014 for channels to 0.035 for vegetated reaches. The model simulation of inundation was conducted using both Newtonian and non-Newtonian closure to determine the effects of non-Newtonian behavior on downstream inundation. The Newtonian and non-Newtonian simulated inundation areas are provided in Figure 19, with the observed inundation boundaries in dark blue. The Newtonian simulations using the post-wildfire hydrology model input interestingly approximates the 100-year floodplain delineated prior to the 2019 debris flow events (FEMA, 2014, 2018), as presented in Kean et al. (2019). The model inundation areas for Montecito and San Ysidro creeks are provided in Figure 20, with simulated model results shown in orange-brown and the observed inundation boundaries shown in blue.

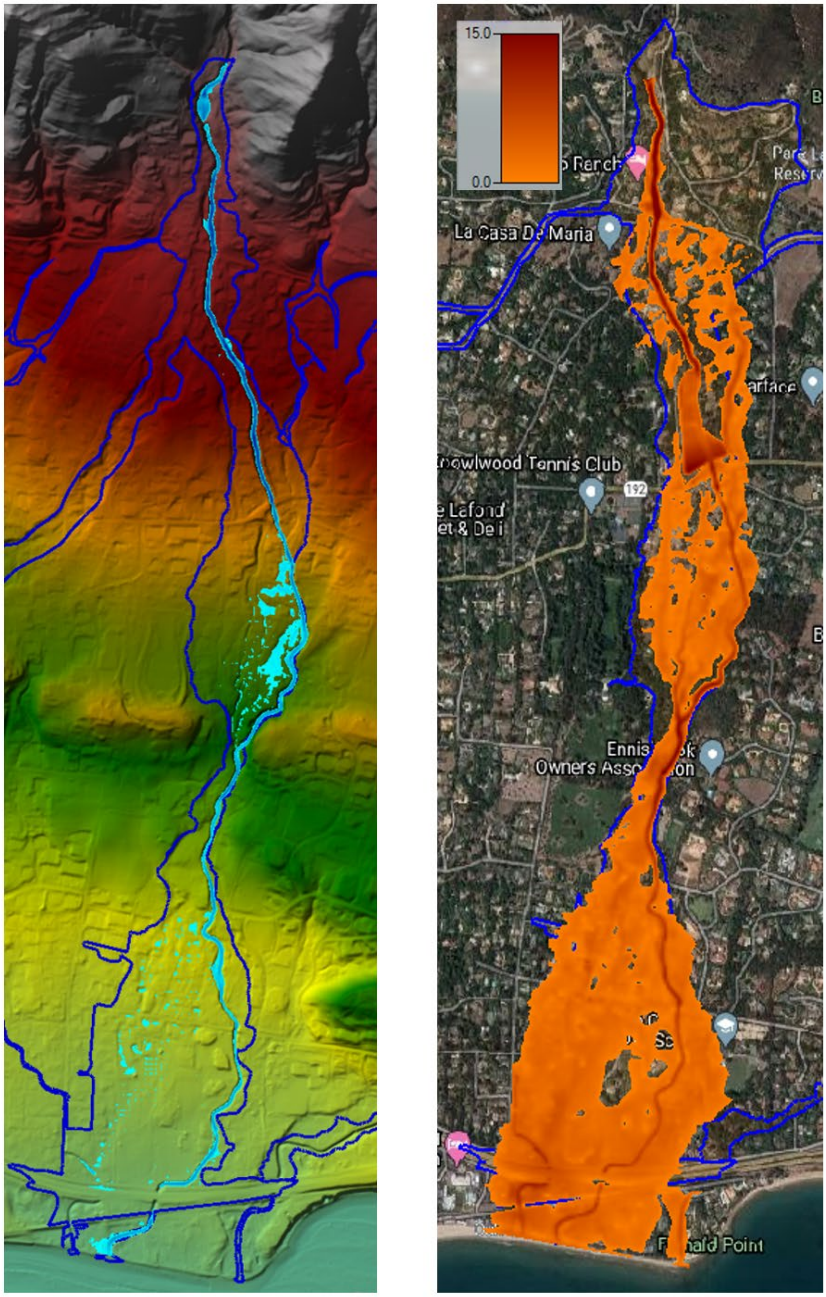

Figure 19. Comparison of Inundation using Newtonian (on left) and Non-Newtonian (on right) modelling approached for San Ysidro Creek. Observed inundation boundaries are shown in dark blue (Kean et al., 2019). Units in feet.

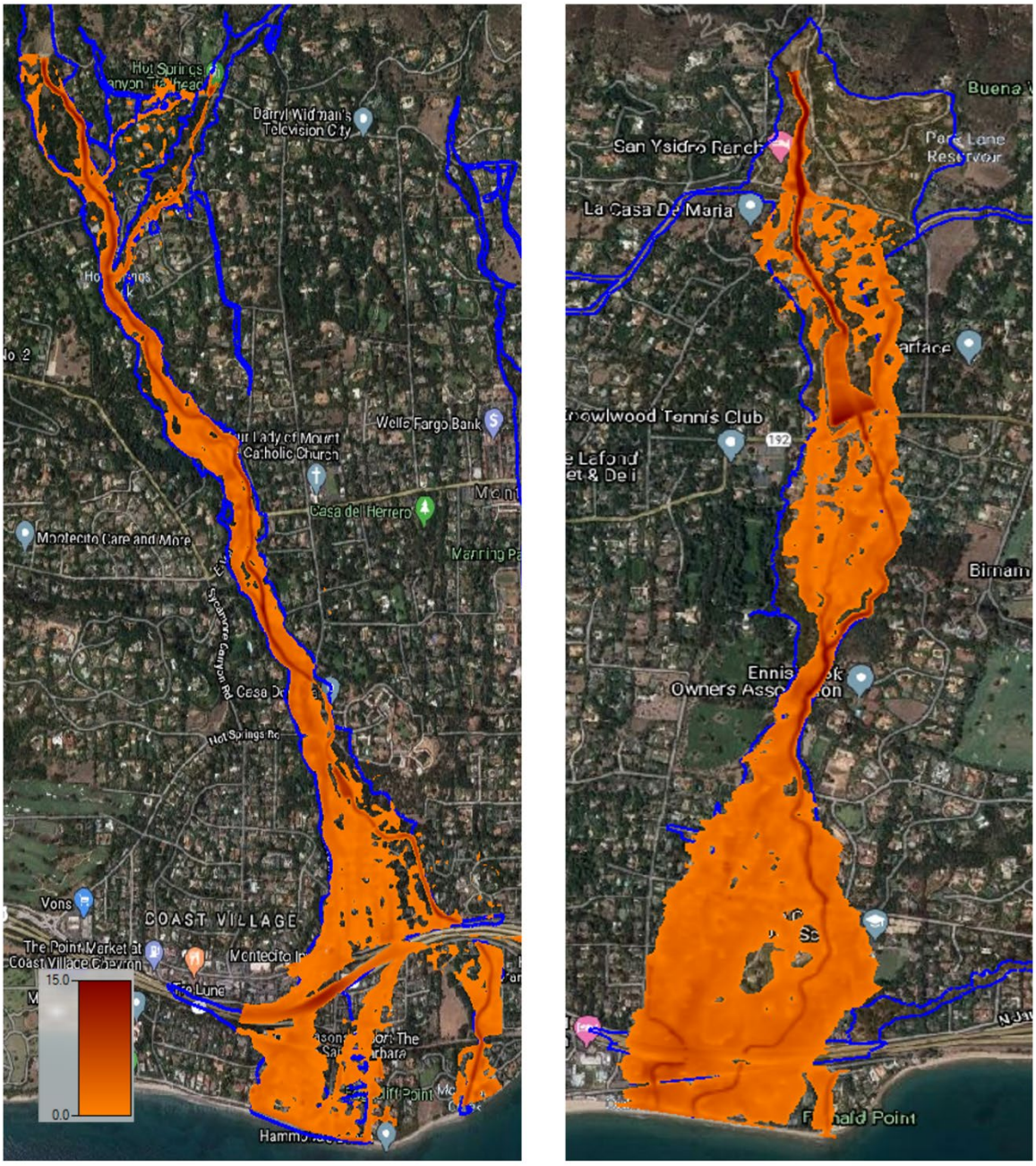

Figure 20. Montecito (on left) and San Ysidro (on right) Inundation Model Results. Same comment: add what dark blue lines are and what the units are for the inundation depth.

Observed velocities are plotted against the computed model results for Montecito and San Ysidro creeks in Figure 21 and Figure 22 below. As anticipated the HEC-RAS model with DebrisLib with the current assumptions would introduce considerable uncertainty. The predicted depths for

Montecito Creek where more consistent with an $R^2 = 0.43$ than the San Ysidro results with an $R^2 = 0.2$.

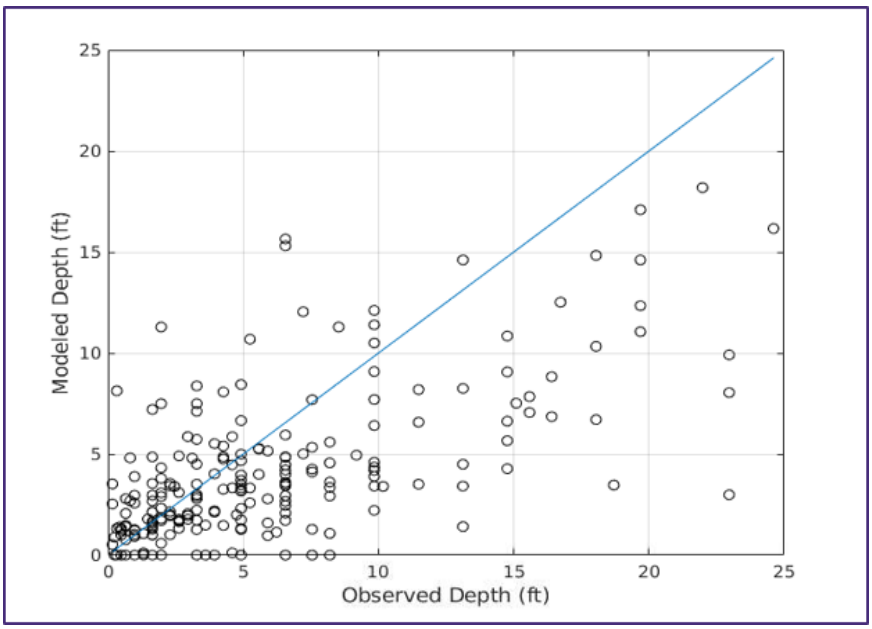

Figure 21. Modelled versus observed depths for Montecito Creek of the 09 January 2018 debris flows.

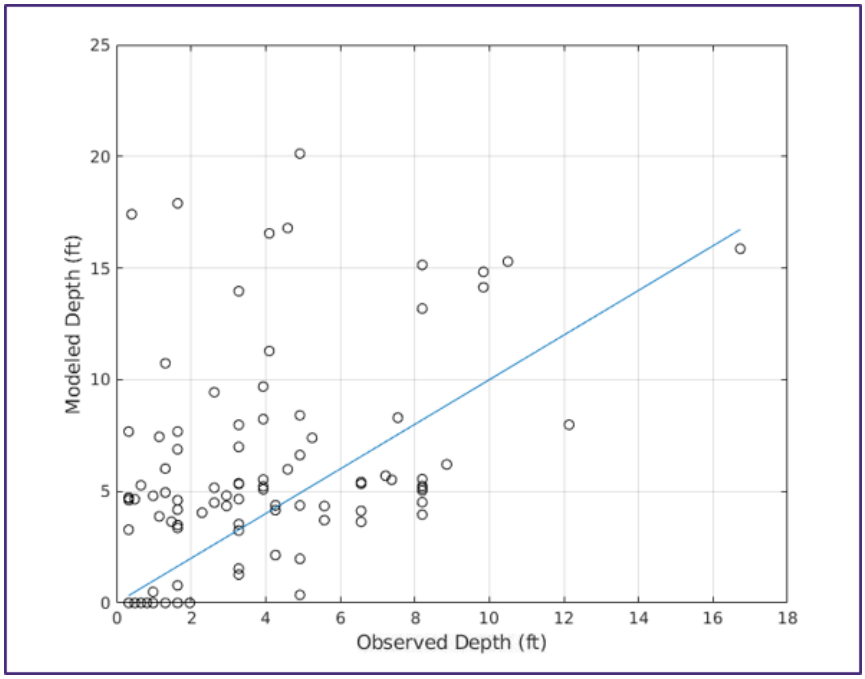

Figure 22. Modelled versus observed depths for San Ysidro Creek of the 09 January 2018 debris flows.

4.6. DISCUSSION AND CONCLUSION

4.6.1. Discussion

The complexity of flow and sedimentation patterns present several challenges when modeling observed data of post-wildfire runoff and inundation. In this work we show how post-wildfire hydraulic simulations that include non-Newtonian processes outperformed the Newtonian-based simulations at predicting depth and inundation with model results diverging from observed depths from Kean et al. (2019). This deviation is most likely a result of the assumptions used here. This limits simulations to a single yield strength and dynamic viscosity across the model domain, which can lead to over or under prediction of depth. Flow depth very sensitive to yield strength and dynamic viscosity. Quantifying the effects of infrastructure (e.g., bridges, culverts) and buildings was important in simulating the approximate flow path within the hydraulic model. The Montecito creek HEC-RAS model included about a 12 bridges and culverts with 9 structures included in the San Ysidro creek model domain. The version of the two-dimensional HEC-RAS code used in this effort was a research version with capabilities for incorporating structures like bridges. Features like bridges and culverts can become blocked and induce avulsion (rapid change in channel flow path). Future research will need to address the challenge of determining how to model this non-Newtonian fluid-structure interaction and sediment deposition and erosion. Regardless, the results and findings presented here indicate the validity of predicting post-wildfire debris flow runout and inundation using a widely-used and -available, engineering software linked with the non-Newtonian DebrisLib.

4.6.2. Conclusion

Watersheds within mountainous wildfire prone areas are at significant risk of damaging post-wildfire floods, debris flows, and sedimentation hazards such as those documented following the 2017 Thomas Fire. Watershed erosion, runoff, and debris flow processes in recently burned areas

are complex and often behave non-linearly with complex feedback mechanisms. Removal of vegetation, alteration of soil structure and properties, reduced surface roughness, and development of water repellant soils result in dramatic changes in hydrology, increased erosion, runoff, and downstream flood risk. Post-wildfire hydrology model and non-Newtonian debris flow models can be used for predicting downstream runout and inundation.

The rheology-based non-Newtonian approaches in DebrisLib improved simulations of measured post-wildfire debris flows following the 2017 Thomas Fire near Santa Barbara, CA. As demonstrated here, the application of non-Newtonian flow approaches with input from calibrated hydrology and empirical debris yield models provide a significant improvement over the current state-of-the-knowledge approaches for modeling post-wildfire flooding (e.g., Bernard, 2007; Cannon et al., 2010; Gartner et al., 2014; Kean et al., 2019). The novel tools presented here allowed for more accurate prediction of the devastating 09 January 2018 debris flow events near Santa Barbara, CA compared to current Newtonian model assumptions. While limitations in the research exist to understand and manage post-wildfire flood hazards, the work presented here enhances the current, widely available, USACE numerical models and tools to assist in preparation for and reducing risks associated with post-wildfire debris flows.

CHAPTER 5. SUMMARY AND RECOMMENDATIONS

5.1. SUMMARY

The research presented here addresses numerical modeling challenges associated with prediction of post-wildfire non-Newtonian flood response within one-dimensional and two-dimensional hydrodynamic numerical models. In mountainous arid and semi-arid regions of the western U.S., wildfires are natural and human induced disasters that can significantly contribute to increased flood risks (DeBano et al., 1998; Neary et al., 2005; Moody et al., 2013). This is further exacerbated by uncertainties in climate change trends, resulting hydrological irregularities, like extreme variations in drought and flood conditions, and wildfires. Post-wildfire flood risk management and restoration have become urgent problems for federal, state, regional and local land management agencies. Which is especially serious in the western U.S. where storms are infrequent but often highly intense and more likely to cause severe damage with increase risks to life, property, and critical infrastructure.

The aim of this research is to establish a physics-based numerical modeling framework to simulate post-wildfire flooding and debris flows to assess the flood risk in downstream communities. The following research questions were partially address during this effort:

1) What are the dominant non-Newtonian processes needed to predict non-Newtonian flow conditions within Newtonian hydrodynamic numerical models? Can a modular non-Newtonian numerical model library approach modify existing current state-of-knowledge shallow-water and diffusive wave Newtonian models?

2) How effective are existing non-Newtonian rheology models (e.g., Bingham, HB, and Quadratic) at predicting non-Newtonian turbulent, transitional, and laminar flow conditions?

3) Can non-Newtonian rheology based models within hydrodynamic models decrease uncertainty in predicting the downstream runoff and inundation and flow variability associated with post-wildfire flood events?

The research is presented in three manuscripts, representing Chapter 2, Chapter 3, and Chapter 4. The first manuscript presents the development and validation of a modular non-Newtonian library that modifies commonly existing diffusive wave and shallow-water based numerical models to account for non-Newtonian behavior commonly documented during post-wildfire flood events. The non-Newtonian library *DebrisLib* validation was conducted using the one- and two-dimensional HEC-RAS models and the two-dimensional AdH numerical model. The non-Newtonian model closure was evaluated with several non-Newtonian flume experiments for a range of gradations, sediment concentration, and flow conditions (laminar, turbulent). The flume experiments included: the Hungr (1995), Haldenwang (2003), and the USGS Large Scale Experiment Flume (Iverson et al., 2010). The companion paper Gibson et al. (2010) extends the *DebrisLib* approach to flume experiments conducted by Parson et al. (2001) for higher concentrated (> 50% volumetric concentration) mudflows and debris flows. Key findings from the research include;

- The results presented here represent the first simulation and validation of non-Newtonian flows within the HEC-RAS and AdH numerical models, two widely used hydrodynamic software packages.

- The modular non-Newtonian model library *DebrisLib* when linked with shallow-water hydrodynamic models can sufficiently replicate a range of non-Newtonian flow conditions. The modular library allows for easy comparison across various numerical models (diffusive wave and shallow water) and reducing uncertainty within a given model approach.
- Both HEC-RAS and AdH when linked with DebrisLib predict the Hungr (1995), Haldenwang (2003), and Iverson et al. (2010) analytical and flume conditions with overall small residuals.
- Even at slopes of 31 degrees (e.g., Iverson et al., 2010) the rheology-based models with HEC-RAS and AdH sufficiently predicted flow depth, velocity, and runout.

Chapter three presents the evaluation and prediction of turbulent and laminar non-Newtonian flow conditions through comparison of Haldenwang (2003) flume experiments against the two-dimensional HEC-RAS and AdH models numerical models linked with modular *DebrisLib*. The aim is to evaluate how effective rheology-based approaches are at predicting turbulent and laminar flows for lower suspended sediment concentrated (or hyperconcentrated) flows. A selection of flume experiments where modeled for 10% concentrated mixtures of kaolinite for a 10-m long, 0.3-m wide flume. Validation was conducted from flume experiment flows and depths, with all rheology closures closely replicated flume results for both HEC-RAS and AdH models. Some key findings from this chapter are;

- All of the non-Newtonian simulations out-performed the Newtonian simulations, adequately predicting discharge and depth (indicating that even at 10% concentration non-Newtonian physics are important).

- The results did deviate from observed conditions at lower discharge conditions, with model results under predicting depth at lower discharges. This is likely a result of the strain rate approximation.
- The rheology-based models predicted both turbulent and transitional flume conditions with very small residuals.
- Limited numerical modeling of Haldenwang (2003) non-Newtonian flume experiments with need for additional research.

The final manuscript presents a hydrology and hydraulic post-wildfire conceptual modeling framework and demonstrates the ability of the non-Newtonian modeling approach presented in Chapters 2 and 3 to predict the post-wildfire flood events following the 2017 Thomas Fire in southern California. This chapter's main goal is to evaluate the non-Newtonian hydraulic modeling of downstream runout and floodplain inundation against data collected by Kean et al., (2019) following the 2018 flood event. The approach was demonstrated using the HEC-HMS hydrology model and the widely used two-dimensional HEC-RAS hydraulic software linked with the *DebrisLib* non-Newtonian library. The approach builds upon existing state-of-practice and attempts to balances the critical need for numerical models to predict post-wildfire flood risk and inundation and uncertainty associated with a limited quantitative understanding of physical processes and modeling. Validated, widely used hydraulic model software with non-Newtonian capabilities (as presented and demonstrated here) will aid the flood risk and engineering community in better managing post-wildfire flood risk. Additional research and wider application of this approach will be needed to evaluate the assumptions and identify the limitations for each. The key findings are presented below:

- The two-dimensional model HEC-RAS with the non-Newtonian *DebrisLib* was able to sufficiently replicate the 09 January 2018 post-wildfire flood event runout and downstream inundation follow the 2017 Thomas Fire.
- The floods behaved almost exclusively as non-Newtonian fluids as presented by Kean et al. (2019) and verified numerically within this study. This is likely the common response in the immediate years following a wildfire.
- The post-wildfire conceptual modeling approach presented here can successfully predict hydrology runoff and downstream flood risk.
- The results indicate that the 100-year floodplain was not a viable metric for predicting post-wildfire flood risk, verifying the similar findings of Kean et al. (2019).
- Current model assumptions that introduce uncertainty include a constant sediment concentration (fixed yield strength and viscosity) and fixed bed conditions. These assumptions introduced limitation in predictions of depth, which was anticipated.
- The increased modeled depth residuals are primarily a function of the constant sediment concentration. This will be addressed in future research by predicting deposition dynamically (a deposition dependent concentration) using non-Newtonian physics with hindered setting.

Some challenges associated with computational modeling of post-wildfire flood and debris flow events include: 1) limited data and poor quantitative understanding of how post-wildfire flood events 'evolve' along the flow path (Newtonian versus Non-Newtonian), 2) predicting post-wildfire flood erosion and deposition processes, and 3) quantifying the effects of infrastructure (e.g., bridges, culvers, buildings, etc.) on non-Newtonian flow and sedimentation, and avulsions. Ongoing and future research will address these limitations.

5.2. RECOMMENDATIONS

Large intense wildfires remove vegetation, destroy soil structure, remove organic matter, reduce surface roughness, and result in the development of hydrophobic soils resulting in dramatic increases in flood magnitude, sediment runoff, and sedimentation. This can persist for years following the wildfire with rill erosion and gully formation driving dramatic downstream sedimentation changes resulting in long-term management concerns. Future research and development will focus on enhancing understanding and modeling capabilities to address post-wildfire flood risk concerns. Some key areas/topics of future research include:

- Efficient and 'real-time' hydrology numerical modeling of post-wildfire flood risk and downstream inundation.
- Simulation of deposition and erosion processes to dynamically predict variable concentration and rheology parameters.
- Evaluation of existing sediment transport modeling approaches to predict non-Newtonian sediment transport processes.
- Better understanding of the longer term geomorphic recovery processes to improve continuous model.
- Development and demonstration of hydrological post-wildfire physical processes and identification of heuristic and physics-based approaches.
- Enhancement of hydraulic numerical modeling approaches presented to address model assumptions and limitations associated with prediction of post-wildfire flood and debris flow events (constant concentration and fixed-bed conditions).
- Develop calibration procedures and ranges of input coefficients.

REFERENCES

Bagnold, R.A., 1954. Experiments on gravity-free dispersion of a large solid sphere in a Newtonian fluid under shear. Proceedings of the Royal Society of London, Series A., Vol. 224, pp. 49-63.

Bagnold, R.A., 1956. Flow of cohesionless grains in fluid. Philosophical Transactions of the Royal Society of London Vol. 249, No. 964, pp. 235-297.

Baldock, T.E., Tomkins, M.R., Nielson, P., and Hughes, M.G., 2004. Settling velocity of sediments at high concentrations. Coastal Engineering, 51(1), p. 91-100.

Berger, R.C, and Howington, S. E., 2002. Discrete Fluxes and Mass Balance in Finite Elements. Journal of Hydraulic Engineering, Vol. 128, No: 1, pp: 87-92.

Bingham, E.C., 1922. Fluidity and plasticity. v. 2, McGraw-Hill.

Burns, K.A., 2007. The effective viscosity of ash-laden flows. Master Thesis, University of Montana, pp. 98.

Cannon, Susan. (2001). Debris-flow generation from recently burned watersheds. Environmental and Engineering Geoscience.p.40

Cannon, Susan & Reneau, Steven. (2000). Conditions for generation of fire-related debris flows, Capulin Canyon, New Mexico. Earth Surface Processes and Landforms - Earth Surf Process Ladnf. p.40

Cannon S.H., and Gartner J.E., 2005. Wildfire-related debris flow from a hazards perspective. In: Debris-flow Hazards and Related Phenomena. Springer Praxis Books. Springer, Berlin, Heidelberg. p.42

Certini, G., 2005. Effects of fire on properties of forest soils: A review. Oecologia, v. 143, p.1-10.

Chen, H., and Lee, C.F., 2000. Numerical simulation of debris flows. Canadian Geotechnical Journal, 37(1), p. 146-160.

Coe, J.A., Kinner, D.A., Godt, J.W., 2008. Initiation conditions for debris flows generated by runoff at Chjalk Cliffs, central Colorado. Geomorphology 96, p. 43

Coussot, Philippe & Meunier, M., 1996. Coussot, P. and M. Meunier. Recognition, classification, and mechanical description of debris flows. Earth Science Review. Earth-Science Reviews. p. 45

Cuthbertson, A., Dong, P., King, S., and Davies, P., 2008. Hindered settling velocity of cohesive/non-cohesive sediment mixtures. Coastal Engineering, 55(12), p. 1197-1208.

Dabak, T., and Yucel, O., 1986. Shear viscosity behavior of highly concentrated suspensions at low and high shear-rates. Rheologica Acta 25, p. 527-533.

DeBano, L.F., Neary, D.G., Folliott, P.F., 1998. Fire's Effects on Ecosystems. John Wiley & Sons, New York 159–196. p.9

Denlinger, R.P. and Iverson, R.M., 2001. Flow of variably fluidized granular masses across three-dimensional terrain. 2. Numerical predictions and experimental tests. Journal of Geophysics Research 106, p. 553–566.

Ebel, B.A., Moody, J.A., and Martin, D.A., 2012. Hydrologic conditions controlling runoff generation immediately after wildfire. Water Resources Research, v. 48, p. 1-13.

Einstein, H.A., and Chien, N., 1955. Effects of heavy sediment concentration near the bed on velocity and sediment distribution. MRD Series, no. 8. Berkeley: University of California: Institute of Engineering Research; Omaha, Nebraska: U.S. Army Engineering Division, Missouri River, U.S. Army Corps of Engineers.

FEMA, 2018, Flood Insurance Rate Maps, Santa Barbara County, California, panels 06083C1392H. p.70

Gabet, E.J., and Sternberg, P., 2008. The effects of vegetation ash on infiltration capacity, sediment transport, and the generation of progressively bulked debris flows. Geomorphology 101, p. 666-673.

Gabet, E. and Simon, M., 2006. The mobilization of debris flows from shallow landslides. Geomorphology. 74. 207-218. p. 42.

Gabet, E., and Bookter, A., 2008. A morphometric analysis of gullies scoured by post-fire progressively bulked debris flows in southwest Montana, USA. Geomorphology. 96. p. 42

Govier, G.W., and Aziz, K., 1972. The flow of complex mixtures in pipes method. Int. J. Multiphase Flow. 8. 83-87. p. 43.

Aziz, K., and George W.G., 1972. Pressure Drop in Wells Producing Oil and Gas. J. Can. Pet Technol., 11: No Pagination Specified. p. 53.

Haldenwang, R., 2003. Flow of non-Newtonian fluids in open channels. p. 53.

HEC 2016. HEC-RAS River Analysis System Hydraulic Reference Manual Version 5.0. February 2016. U.S. Army Corps of Engineers Hydrologic Engineering Center, CPD-69.

Hergarten, S., and Robl, J., 2015. Modelling rapid mass movements using the shallow water equations in Cartesian coordinates. Nat. Hazards Earth Syst. Sci. v. 15 p. 671–685.

Hungr, O., 1995. A model for the runout analysis of rapid flow slides, debris flows, and avalanches. Canadian Geotechnical Journal 32(4) p. 610-623.

Hungr, O., 2005. Classification and terminology. In: Hungr O, Jakob M (eds) Debris-flow hazards and related phenomenon. Praxis Publishing Ltd., Chichester. p. 15

Imran, J., Parker, G., Locat, J., and Lee, H., 2001. 1D numerical model of muddy subaqueous and subaerial debris flows. Journal of Hydraulic Engineering, 127, p. 959-968

Iverson, R.M., 1997. The physics of debris-flows. Reviews of Geophysics, American Geophysical Union 35(3), p. 245-296.

Iverson, R.M., and Denlinger, R.P., 2001. Flow of variably fluidized granular masses across three-dimensional terrain: 1. Coulomb mixture theory. Journal of Geophysical Research 106, p. 537-552.

Iverson, R.M., Logan, M., LaHusen, R.G., and Berti, M., 2010. The perfect debris flow? Aggregated results from 28 large-scale experiments. Journal of Geophysical Research 115, F03005.

Jeyapalan, K., 1981. Analysis of flow failures of mine tailing impoundments. PhD Thesis, University of California, Berkeley.

Jin, M., and Fread, D.L., 1997. 1D Modeling of Mud/Debris unsteady flows. Journal of Hydraulic Engineering, 125(8), p. 827-834.

Johnson, A.M., and Rodine, J.R., 1984. Slope instability. Wiley 535, p. 257-361.

Julien, P.Y., and Lan, Y., 1991. Rheology of Hyperconcentrations. Journal of Hydraulic Engineering 115, no. 3, p. 346-353.

Julien, P.Y., 2010. Erosion and Sedimentation. Cambridge University Press 2nd Eds., pp. 371.

Lane, P.N.J., Sheridan, G.J., and Noske, P.J., 2006. Changes in sediment loads and discharge from small mountain catchments following wildfire in south eastern Australia. Journal of Hydrology 331, p. 495-510.

Luna, Q.B., Remaitre, A., van Asch, Th. W.J., Malet, J.-P., and van Westen, C.J., 2012. Analysis of debris flow behavior with a one dimensional run-out model incorporating entrainment. Engineering Geology, 128, p. 63-75.

Major, J.J., and Pierson, T.C., 1992. Debris flow rheology: experimental analysis of fine-grained slurries. Water Resource. Res. 28 (3), 841–857 p. 42.

Martinez, C., Miralles-Wilhem, F., and Garcia-Martinez, R., 2007. A 2D finite-element debris-flow model based on the Cross rheology formulation. In: C. Chen and J. Major (Eds.), Debris-flow hazard mitigation: mechanics, prediction, and assessment. Millpress, Netherlands, p. 189-196.

McArdell, B.W., Bartelt, P., and Kowalski, J., 2007. Field observations of basal forces and fluid pore pressure in a debris flow. Geophysical Research Letters, Vol. 34, pp. 1-4.

Meyer, G.A., Wells, S.G., 1997. Fire-related sedimentation events on alluvial fans, Yellowstone National Park, U.S.A Journal of Sedimentary Research 67, 776–791. p. 42

Moody, J.A., Kinner, D.A., and Ubeda, X., 2009. Linking hydraulic properties of fire affected soils to infiltration and water repellency. Journal of Hydrology, v. 379, p. 291-303.

Moody, J.A., Shakesby, R.A., Robichaud, P.K., Cannon, S.H., and Martin, D.A., 2013. Current research issues related to post-wild wildfire runoff and erosion processes. Earth-Science Reviews 122, p. 10-37.

Mooney, M. (1931). Explicit Formulas for Slip and Fluidity. Journal of Rheology 2: 210-222. p. 43.

Naef, D., Rickenmann, D., Rutschmann, P., and Mcardell, B.W., 2006. Comparison of flow resistance relations for debris flows using a one-dimensional finite element simulation model. Natural Hazards and Earth Systems Science, 6(1), p. 155-165.

Naik, B., and Jerry, D.H., 1983. Mechanics of Mudflows Treated as the Flow of a Bingham Fluid. Washington. p. 53

Neary, D.G., Ryan, K.C., and DeBano, L.F., 2005. Wildland fire in ecosystems: effects of fire on soil and water. USDA Forest Service, Rocky Mountain Research Station, General Technical Report, RMRS-GRT-42-Volume 4, Ogden, UT.

NSTC, 2015. Wildland fire science and technology task force final report. Committee on Environment, Natural Resources, and Sustainability Subcommittee on Disaster Reduction, National Science and Technology Council, November 2015, 28 pp.

O'Brien, J.S., Julien, P.Y., and Fullerton, W.T., 1993. Two dimensional water flood and mudflow simulation. Journal of Hydraulic Engineering 119(2), p. 244-261.

Orem, C.A., and Pelletier, J.D., 2016. The predominance of post-wildfire erosion in the long-term denudation of the Valles Caldera, New Mexico. Journal of Geophysical Research: Earth Surface, Vol. 121, pp. 843-864.

Parise, M., and Cannon, S., 2012. Wildfire impacts on the processes that generate debris flows in burned watersheds. Natural Hazards. p. 40

Parson, J.D., Whipple, K.X., and Simoni, A., 2001. Experimental study of grain-flow, fluid-mud transition in debris flows. Journal of Geology 109, p. 427-447.

Perez, C.M., 2017. CFD modelling of laminar, open-channel flows of non-Newtonian slurries. Master's Thesis, University of Alberta. 146 pp.

Phillips, C.J., and Davies, T.R.H., 1991. Determining rheological parameters of debris flow material. Geomorphology 4, 101–110. p.45

Pierce, J.L., Meyer, G.A., and Jull, A.J.T. (2004). Fire-induced erosion and millennial-scale climate change in northern ponderosa pine forests. Nature, Vol 423, pp. 87-90.

Pradhan, N.R., Floyd, I.E., Downer, C., Gibson, S., and Heath, R.E., 2019. Newtonian and Non-Newtonian sediment fluid flow hydrodynamic runoff model. SEDHYD 2019 Conference Paper, pp. 13.

Pudasaini, S.P., Wang, Y., and Hutter, K., 2005. Modelling of debris flows downs general channels. Natural Hazards and Earth Systems Science, 5(6), p. 799-819.

Richardson, J.F., and Zaki, W.N., 1954. Sedimentation and fluidization: part 1. Transactions of Institution of Chemical Engineers 32, p. 35-53.

Rowe, P.B., Countryman, C.M., and Storey, H.C., 1954. Hydrologic analysis used to determine effects of fire on peak discharge and erosion rates in southern California watersheds. USDA Forest Service, California Forest and Range Experimental Station, pp. 49.

Savage, S.B., and Hutter, K., 1989. The motion of a finite mass of granular material down a rough incline. Journal of Fluid Mechanics, 199, p. 177-215.

Savant, G., Trahan, C.J. and McAlpin, T.O., 2019. Streamline Upwind Petrov-Galerkin (SUPG) Based shallow water model for large scale geophysical flows in Cartesian and Spherical coordinates. Journal of Waterways, Ports and Coasts, Vol: 145, No: 5.

Savant, G., Trahan, C.J., Pettey, L., McAlpin, T.O., Bell, G.L. and McKnight, C.J., 2018. Urban and overland flow modeling with dynamic adaptive mesh and implicit diffusive wave equation solver. Journal of Hydrology, Vol. 573, pp: 13-30.

Savant, G., Trahan, C.J., Berger, R.C., McAlpin, J.T. and McAlpin, T.O., 2018. Refinement Indicator for Dynamic Mesh adaption in Three-Dimensional Shallow Water Equation Modelling. Journal of Hydraulic Engineering. Vol: 144, No: 2, published online: November 16, 2017.

Savant, G., Berger, R.C., McAlpin, T.O. and Tate, J.N., 2011. Efficient Implicit Finite-Element Hydrodynamic Model for Dam and Levee Breach. Journal of Hydraulic Engineering, Vol. 137, No. 9

Shakesby, R.A., 2011. Post-wildfire soil erosion in the Mediterranean: review and future research directions. Earth-Science Reviews 105, p. 71-100.

Shakesby, R.A., and Doerr, S.H., 2006, Wildfire as a hydrological and geomorphological agent: Earth-Science Reviews, v. 74, p. 40.

Shakesby, R.A., Coelho, C.O.A., Ferreira, A.D., Terry, J.P., and Walsh, R.P.D., 1993. Wildfire impacts on soil erosion and hydrology in wet Mediterranean forest, Portugal. International Journal of Wildland Fire 3, p. 95-110.

Shin, S.S., 2010. Response of runoff and erosion with vegetation recovery in differently treated hillslopes after forest fire, Korea. 8th International Symposium on Ecohydraulics, Seoul, Korea, September 2010.

Takahashi, T., 1978. Mechanical characteristics of debris-flows. Journal of Hydraulic Engineering 104, p. 381-396.

Takahashi, T., 1980. Debris flow on prismatic open channel. Journal of the Hydraulics Division, 106(3), pp.381-396.

Takahashi, T., Nakagawa, H., Harada, T. and Yamashiki, Y., 1992. Routing debris flows with particle segregation. Journal of Hydraulic Engineering, 118(11), pp.1490-1507.

Trahan, C.J., Savant, G., Berger, R.C., Farthing, M., McAlpin, T.O., Pettey, L., Choudhary, G.K. and Dawson, C.N., 2018. Formulation and application of the adaptive hydraulics three-dimensional shallow water and transport models. Journal of Computational Physics, Vol: 374, published online: August 7, 2018, pp: 47-90.

Wilson, K. C. and Thomas, A.D., (1985). A new analysis of the turbulent flow of non-Newtonian fluids. Canadian Journal of Chemical Engineering 63 539-546. p. 43.

VITA

Ian Eli Floyd, born in Hattiesburg, Mississippi, grew up nearby in Magee, Mississippi and was a member of the U.S. Army and Air Force serving for over a decade. He received his bachelor's and master's degree in Geology from the University of Southern Mississippi and began working at U.S. Army Engineer Research and Development Center (ERDC) in Vicksburg, Mississippi. As his interest in science and engineering grew, he decided to enter the Department of Civil and Environmental Engineering at Louisiana State University. Upon completion of his doctoral degree, he will continuing conducting research at U.S. Army ERDC.